Energy Research and Development Division
FINAL PROJECT REPORT

SUPPORT OF U.S. DEPARTMENT OF ENERGY CONTRACT FOR NOVEL CONTROL OF COMBINED COOLING, HEATING AND POWER SYSTEMS

Prepared for: California Energy Commission
Prepared by: Advanced Power and Energy Program
University of California, Irvine

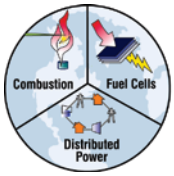

ADVANCED POWER & ENERGY PROGRAM
UNIVERSITY of CALIFORNIA · IRVINE

JANUARY 2017
CEC-500-2017-002

PREPARED BY:

Primary Author(s):
Li Zhao
Jacob Brouwer

Advanced Power and Energy Program
University of California, Irvine
221 Engineering Laboratory Facility
Irvine, California 92697-3550
Phone: 949-824-1999 | Fax: 949-824-7423
http://www.apep.uci.edu

Contract Number: 500-10-010

Prepared for:

California Energy Commission

Mike Kane
Contract Manager

Aleecia Gutierrez
Office Manager
Energy Generation Research Office

Laurie ten Hope
Deputy Director
ENERGY RESEARCH AND DEVELOPMENT DIVISION

Robert P. Oglesby
Executive Director

PREFACE

The California Energy Commission Energy Research and Development Division supports public interest energy research and development that will help improve the quality of life in California by bringing environmentally safe, affordable, and reliable energy services and products to the marketplace.

The Energy Research and Development Division conducts public interest research, development, and demonstration (RD&D) projects to benefit California.

The Energy Research and Development Division strives to conduct the most promising public interest energy research by partnering with RD&D entities, including individuals, businesses, utilities, and public or private research institutions.

Energy Research and Development Division funding efforts are focused on the following RD&D program areas:

- Buildings End-Use Energy Efficiency
- Energy Innovations Small Grants
- Energy-Related Environmental Research
- Energy Systems Integration
- Environmentally Preferred Advanced Generation
- Industrial/Agricultural/Water End-Use Energy Efficiency
- Renewable Energy Technologies
- Transportation

Support of U.S. Department of Energy Contract for Novel Control of Combined Cooling, Heating, and Power Systems is the final report for the Support of U.S. Department of Energy Contract for Novel Control of Combined Cooling, Heating and Power Systems project (contract number CEC-10-010) conducted by Advanced Power and Energy Program, University of California, Irvine. The information from this project contributes to Energy Research and Development Division's Buildings End-Use Energy Efficiency Program. Any unattributed materials (e.g., tables and figures) are produced by the UCI research team.

When the source of a table, figure or photo is not otherwise credited, it is the work of the author of the report.

For more information about the Energy Research and Development Division, please visit the Energy Commission's website at www.energy.ca.gov/research/ or contact the Energy Commission at 916-327-1551.

ABSTRACT

This report presents the physical models developed for the project *Support of U.S. Department of Energy Contract for Novel Control of Combined Cooling, Heating and Power Systems*. The models were built in the MATLAB-Simulink® framework using a methodology developed by the University of California Irvine (UCI). In addition, the project team developed and verified these economic and environmental analyses strategies and models used in the project: Photovoltaic Model, Lead-acid Battery Model, Lithium-ion Battery Model, Ultra-capacitor Model, Heat Recovery Steam Generator Model and Steam Turbine Model.

Dynamic data for buildings was collected and analyzed and the team also acquired a large amount of data from the UCI Central Plant demonstration of the novel controls and optimization software and hardware installed at the UCI Central Plant.

The original control algorithms and architectures were also demonstrated in the Engineering Laboratory Facility of the University of California, Irvine and the UCI central plant. The control algorithms were translated to Siemens controls and installed to demonstrate the novel control algorithms for economical dispatch of a CCHP system.

Keywords: CCHP, Economic Dispatch, Control Strategy, Energy Cost

Please use the following citation for this report:

Zhao, Li; Jacob Brouwer. (Advanced Power and Energy Program, University of California, Irvine). 2016. ***Support of US Department of Energy Contract for Novel Control of Combined Cooling, Heating, and Power Systems.*** California Energy Commission. Publication number: CEC-500-2017-002.

TABLE OF CONTENTS

LIST OF FIGURES

LIST OF TABLES

EXECUTIVE SUMMARY

Introduction

Combined cooling, heating and power (CCHP) technology can support large energy efficiency improvements and significant reductions of greenhouse gas (primarily CO_2) emissions. While CCHP has been significantly applied in large applications (greater than 20 megawatts), the smaller commercial and industrial applications between 500 kilowatts and 5 megawatts (MW) have not been fully exploited. Various estimates of the CCHP market potential in the industrial sector are between 30-90 gigawatts (GW) of electrical capacity. The "light" industrial market (0.5 – 5MW of electrical capacity) comprises about 60 percent of the total industrial CCHP market potential. In addition, similar applications of CCHP in the commercial and institutional market sectors are estimated to comprise about 75 GW of the market potential. As a result, the combined light industrial, commercial and institutional CCHP market potential ranges from 93 to 129GW.

However, CCHP in the smaller commercial and industrial applications are currently challenged by numerous barriers and include those generally categorized as product performance and availability barriers, awareness, information and education barriers, utility policies and regulatory barriers, planning, siting and zoning barriers, environmental regulation, and supporting market infrastructure barriers. Among these barriers are three high priority challenges that must be overcome to adopt the light industrial, commercial and institutional CCHP. These high priority challenges are:

1. Lack of cost-competitive equipment options in the appropriate size range (0.5 – 5MW)
2. Lack of information on the value of these smaller systems for potential users
3. Lack of controls sufficient to deal with the highly dynamic nature and relative non-coincidence of the thermal and electrical loads in many of these applications

The current research and development effort directly addresses these challenges and significantly contributes to increased CCHP market penetration in the light industrial, commercial and institutional sectors.

Project Purpose

Most commercial and industrial electrical loads are highly dynamic and typically not synchronized with local heating and cooling demands. These dynamics, together with utility charges and non-export requirements, often make CHP (Combined Heating and Power)/ CCHP systems less cost effective and less attractive to end-users.

A new, dynamic CHP/CCHP system control approach is required to address this issue and overcome the barriers. The current research and development effort directly addresses these challenges to develop innovative control strategies for dynamic economical dispatch of CHP/CCHP systems with emissions constraints and thermal load following capability. This new CHP/CCHP control technology will significantly contribute to increased CHP/CCHP market penetration in California's light industrial, commercial and institutional sectors. The

new control algorithms and technology were developed based on previous research, experience and expertise at UCI, and directly addresses the high priority challenges in a variety of applications.

Project Process and Results

This project developed dynamic models for selected CCHP components and integrated systems technologies to support a parallel project funded by the U.S. Department of Energy which is also developing novel controls for CCHP systems. Researchers built the models in the MATLAB-Simulink® framework using a methodology developed by researchers at UCI as well as, developed the economic and environmental analyses strategies and models that were used in the project. UCI developed a dynamic model for each of the primary system components, and then interconnected the components together to represent the CCHP system. The system dynamic models are subjected to dynamic CCHP load demands and other distresses. This allows the dynamics of individual components as well as interactions among system components to simulate the system dynamic response. All of the dynamic models are presented - Photovoltaic Model,Lead-acid Battery Model, Lithium-ion Battery Model, Ultra-capacitor Model, Heat Recovery Steam Generator Model and Steam Turbine Model.

CCHP systems can provide many benefits over traditional central generation such as increased reliability and efficiency while reducing emissions. Despite these potential benefits, a CCHP system is generally not purchased unless it reduces energy costs. Economic dispatch strategies can be designed so the CCHP technologies reduce overall facility energy costs. The researchers collected and analyzed building dynamic and central plant data so several industrial and commercial facilities could be simulated using the electrical, heating, and cooling load data. Industrial and commercial utility rate structures were modeled after Southern California Edison and Southern California Gas Company tariffs and used to establish energy costs for the simulated buildings. Using these control strategies, building models, and utility rate models, a study examining various generator characteristics is performed.

The project team developed and tested innovative control algorithms and architecture to demonstrate a microturbine generator in the Engineering Laboratory Facility of UCI. The control algorithms were translated to Siemens controls and installed to demonstrate the new control algorithms for economical operation of a CCHP system.

Project Benefits

The results from this research, development and demonstration project provided a detailed understanding of the dynamic performance characteristics of CHP/CCHP systems and system components required to control these integrated systems under economic and environmental constraints. The models, algorithms, and control strategies described enable developers, installers and end-users to duplicate these efforts and deploy CHP/CCHP to a broader range of applications which have been underserved because of economic or environmental considerations.

The project supports the PIER goal to develop, and help bring to market, energy technologies that provide increased environmental benefits, greater system reliability, and lower system

costs. The current effort provided tangible benefits to electric utility customers with the development of advanced controls for electricity generation technologies that exceed applicable standards and increase reductions in greenhouse gas emissions from electricity generation. The current effort will also lead to greater adoption of advanced electricity technologies that reduce the consumption of fossil fuels. Specifically, the advanced innovative controls make CHP/CCHP systems more capable of meeting demands for a larger cross-section of the potential market and make market adoption of CHP/CCHP technology more rapid. Increasing the market potential and market adoption of CHP/CCHP technology will provide California ratepayers with these benefits:

- Lower energy use (improved fuel use efficiency) by 10.4 to 31.2TBtu/year contributing to conservation of limited primary energy resources
- Reduced criteria pollutants by 177 to 531 metric tons per year leading to improved air quality
- Reduced greenhouse gas emissions by roughly 0.63 to 1.89 million metric tons annually, contributing to meeting state goals for GHG reduction and lessens impacts on the global climate
- Lower ultimate cost of electricity and heat than would otherwise result due to energy that is saved and due to the increasing costs of emissions

CHAPTER 1:
Development and Verification of First Principles Dynamic Physical Models of Emerging CCHP Technologies

While the market potential and emissions reductions of Combined Cooling, Heat and Power (CCHP) use are significant, CCHP use is currently challenged by a host of barriers. The general problem is that, although CCHP technology could significantly contribute to reductions in energy use, criteria pollutant and greenhouse gas emissions, market adoption and installation of CCHP technology is too slow. Contributing broadly to this fact and directly related to the general technical and market barriers listed above are three priority challenges that must be overcome to enable higher adoption of CCHP technology. These barriers include 1) Lack of cost-competitive options in the appropriate size range, 2) Lack of information on the value of these systems for potential users, and 3) Lack of controls sufficient to deal with the highly dynamic nature and relative non-coincidence of the thermal and electrical loads in many applications. The specific problem is that most commercial and industrial electrical loads are highly dynamic and typically not synchronized with local heating and cooling demands. These dynamics, together with utility charges and non-export requirements often make CCHP systems less cost effective and less attractive to end-users.

To address these barriers, researchers at the University of California, Irvine (UCI) developed a new, dynamic CCHP system model and control approach to better align CCHP performance with user and utility requirements. As a first step, the project team developed and verified first principles dynamic physical models for emerging CCHP technologies.

This chapter summarizes the model development effort and describes in detail each of the models developed therefrom. This chapter is organized by technology in the following sections: Photovoltaic Model,Lead-acid Battery Model, Lithium-ion Battery Model, Ultra-capacitor Model, Heat recovery steam generator Model and Steam Turbine Model.

1.1 Photovoltaic Model

1.1.1 Model Description

Solar photovoltaic (PV) electricity sources convert sunlight directly into electricity through the use of semiconductor technology. Sunlight is composed of photons that have energy (E) proportional to their frequency (f) according to E = hf, where h is Planck's constant. When the photon hits a semiconductor, it will either be reflected or transfer its energy to the surface. If this energy is greater than the band gap of the material, an electron will be promoted from the valence band to the conduction band. In this way, the heart of a PV cell is a current source: photons strike a surface to emit electrons. This in itself will not produce electricity, as without the presence of an electric field, the electron will fall back into the 'hole' created by its absence. However, the silicon material can be doped with atoms that have either three (p-type) or five (n-type) valence electrons. The lattice structure of silicon is achieved with four valence electrons, so

the addition of an n-type impurity will cause four of those electrons to participate in the lattice structure and leave one essentially 'free' electron. Similarly, a p-type dopant will create a hole. Both these materials are electrically neutral, but due to the structure, when put together, the free electrons tend to migrate to the holes, which creates an intrinsic electric field in the material that is called a p-n junction. Now, when a photon strikes the semiconductor, the electron will have the force of an electric field and provide current[1]. However, this p-n junction also creates a diode in parallel with the current source that must be accounted for in the PV model. The resistance of the current through the semiconductor material and contacts creates a series resistance with the current source and diode as well. Thus the simplest PV cell model is presented with current source, diode, and resistance in Figure 1.

Figure 1: Simple Electric Schematic of a Solar PV Cell

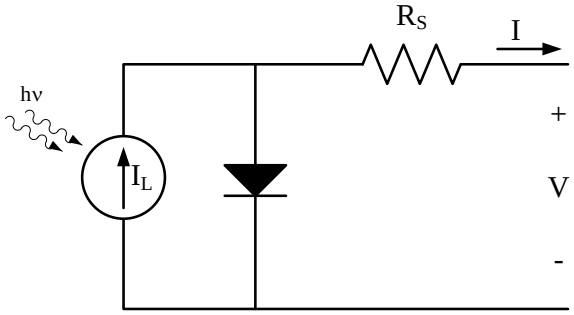

1.1.1.1 Irradiation Module

Solar power-producing devices such as photovoltaics are capable of producing electrical power from both direct and indirect light inputs. Therefore, the total irradiation that is incident on the photovoltaic cell must be calculated from the different irradiation components. Calculation of the in-plane irradiation on the solar array is done using the exact model constructed by Heling[2]. The model reads files containing hourly data for different types of solar insolation for a given location: Direct "beam" insolation (B) is the component of the sun's radiation which arrives on a horizontal surface at ground level without interruption, in a straight line from the sun. Indirect "diffuse" insolation (D) is the component of the sun's radiation which arrives at a horizontal surface at ground level after being reflected from atmospheric objects such as clouds and airborne particles. An additional given parameter is the global horizontal irradiation (H), which is the amount of total (beam and diffuse) irradiation striking a horizontal surface at ground elevation. The model uses the different insolation types to calculate in-plane beam irradiation

[1]J. J. Kraushaar and R. A. Ristinen, **Energy and Problems of a Technical Society**, 2nd ed: John Wiley & Sons, 1993.

[2]M. G. Heling, **Assesment of the Zero-Emission Vehicle, Shared-Use Station Car (Zev-Susc) Mobility Concept With a Focus on Energy and Environmental Sustainability**, Master thesis, University of California, Irvine, 2008.

(I_b), the in-plane diffuse irradiation (I_d), and the in-plane irradiation that is reflected from the ground (I_r). The total in-plane irradiation on the solar panel is then:

$$I = I_b + I_d + I_r$$

The in-plane beam irradiation is calculated according to the following method using the solar declination and the true solar time. The solar declination (δ), which is the angle between the earth's equatorial plane and a straight line drawn between the center of the earth and the center of the sun, is calculated for locations north of the equator as:

$$\delta = 23.45^{\circ} \sin\left[\frac{360(d_n + 284)}{365}\right]$$

Where d_n is the serial number of the day of the year. The true solar time, which is the difference between noon and the considered hour of the day in terms of a complete revolution of the earth, is calculated as:

$$\omega = 15 \times (TO - AO - 12) - (LL - LH)$$

where TO is the local time, AO is the time by which the clocks are advanced ahead of local time zones, LL is the longitude of the site in consideration, and LH is the reference longitude of the local time zone encompassing the site in consideration. Note that TO and AO are in hours, and LL, LH are in degrees.

The solar declination and true solar time used to calculate the angle of solar incidence θ_s, which is the angle between the sun and the line that perpendicular to the face of the photovoltaic array, calculated as:

$$\cos\theta_s = \sin\delta \sin\phi \cos\beta - \sin\delta \cos\phi \sin\beta \cos\alpha + \cos\delta \cos\phi \cos\beta \cos\omega + \ldots$$

$$\cos\delta \sin\varphi \sin\beta \cos\alpha \cos\omega + \cos\delta \sin\alpha \sin\omega \sin\beta.$$

where ϕ corresponds to the latitude of the site under consideration.

The total in-plane beam irradiation is then calculated by:

$$I_b = B \max(0, \cos\phi_s)$$

The total in-plane reflected irradiation can also be calculated by:

$$I_r = \rho_g H \frac{1 - \cos\beta}{2}$$

Where ρ_g is the reflectivity of the ground? The in-plane diffuse irradiation is calculated according to the model presented by Perez[3], represented by:

$$\theta_Z = \cos\phi\cos\delta\cos\omega + \sin\phi\sin\delta$$

$$I_d = D\left[\frac{(1-F_1)(1+\cos\beta)}{2} + F_1\frac{a}{b} + F_2\sin\beta\right]$$

Where F_1 and F_2 are functions of the sky condition3, and θ_Z is the solar zenith angle as calculated[4]. The values for a and b are calculated according to:

$$a = \max(0, \cos\theta_S)$$

$$b = \max(0.087, \cos\theta_Z)$$

1.1.1.2 Fixed-Plate Solar Photovoltaic Module

The PV model captures the effect of solar irradiance, cloud cover, and ambient temperature on the array output power, dynamically capturing the intermittent nature of solar PV power. The model integrates (1) an equivalent circuit model for power output and (2) an energy balance based PV cell temperature model. The developed model is tuned to represent experimentally measured data of a Solarex MSX-60 panel installed on top of the Engineering Laboratory Facility at the University of California, Irvine. The developed module model output is scaled to simulate any sized solar installation parametrically.

The Power Block model was developed based on an equivalent circuit representation of a solar cell as presented by Walker[5], with temperature dependence of the diode saturation current (I_o) and photo-current (I_L), and the inclusion of a series resistor.

The current output of the PV cell is equal to the difference between the current source (I_L) and the diode current (I_D). The diode current can be expressed according to the Shockley equation, which is presented in the following Equation.

$$\boldsymbol{I_D = I_O\left(e^{V_D/nV_T} - 1\right)}$$

Where I_0 is the reverse bias saturation current and V_T is the thermal voltage $V_T = kT/q$. For the thermal voltage, k is the Boltzmann constant, T is temperature in Kelvin, and q is the elementary charge of an electron. V_D is the voltage across the diode, and n is a quality factor of the semiconductor, generally between 1 and 2 with 1.2 used herein5.

---

[3] R. Perez and P. Ineichen, **Modeling Daylight at Availability and Irradiance Components From Direct and Global Irradiance.** Solar Energy, 1990. 44(5): p. 271-289.

[4] J. A. Duffie and W. A. Bechman, **Solar Engineering of Thermal Processes**, John Wiley & Sons, 1991.

[5] G. Walker, Evaluating MPPT Converter **Topologies Using a MATLAB PV Model**, Journal of Electrical and Electronics Engineering, Australia, vol. 21, pp. 49-55, 2001.

Thus, the overall current produced by the PV cell is:

$$I = I_L - I_O\left(e^{q(V+IR_s)/nkT} - 1\right)$$

The current source photo-current, I_L, is directly proportional to irradiance, G. The photo-current is generally constant for a specific irradiance and temperature and has a linear dependence with temperature. The equation for photo-current at any irradiance and temperature is thus5:

$$I_L = \frac{G * I_{SC(T_1,nom)}}{G_{(nom)}}\left(1 + K_0 \frac{(T - T_1)}{(T_2 - T_1)}\right)$$

$$K_0 = \frac{\left(I_{SC(T_2)} - I_{SC(T_1)}\right)}{I_{SC(T_1)}}$$

The reverse bias saturation current, I_0, is shown below from[6].

$$I_0 = I_{0(T_1)} * \left(\frac{T}{T_1}\right)^{3/n} * e^{-qV_g/\left(nk\left(\frac{1}{T} - \frac{1}{T_1}\right)\right)}$$

$$I_{0(T_1)} = I_{SC(T_1)}/\left(e^{qV_{OC(T_1)}/nkT_1} - 1\right)$$

Which can be evaluated directly with known constants and from values on the data sheet. The specific panel modeled here is the Solarex MSX-60 PV panel, which is a 60W panel comprised of 36 series-connected cells. The array open circuit voltage (VOC), at 25°C is 21.0V, and the short circuit current, I_{SC}, is 3.74 A. The I_{SC} increases to 3.92 A at 75°C. The Rs is found to be about 8mΩ5.

Cell Temperature Block: The temperature of the solar cell is determined by applying conservation of energy to a control volume encompassing the entire 5 kW solar array. Heat transfer due to convection and radiation was resolved, however conduction was assumed to be negligible since the contact area of the panel interconnects with the roof is very small:

$$\rho \forall C_v \frac{dT_s}{dt} = Q_{rad} - Q_{conv} - Q_{rad,loss} - W$$

Convective heat transfer was determined using a turbulent-flow Nusselt number approach for a flat plate:

$$\overline{Nu} = \frac{\overline{h}L}{k_f} = 0.664\,\mathrm{Re}_L^{0.5}\,\mathrm{Pr}^{0.33}$$

Where Re_L is the Reynolds number of the ambient flow, Pr is the Prandtl number, k_f is the thermal conductivity of the ambient air, L is the length of the plate, and A_s is the surface area of

[6]J. A. Gow and C. D. Manning, **Development of a Photovoltaic Array Model For Use in Power-Electronics Simulation Studies**, Electric Power Applications, IEE Proceedings -, vol. 146, pp. 193-200, 1999.

the array. For the case of the solar panel, the length of the plate is taken to be the diagonal of the panel area.

The density, dynamic viscosity, thermal conductivity and Prandtl number are temperature dependent. The velocity of the ambient air is taken from measured wind speed data in the Santa Ana region for the appropriate time period.

Radiative heat transfer was modeled using the grey body assumption, where the temperature of the grey surface is set to the ambient temperature:

$$Q_{rad} = \left(G_{measured} - \varepsilon\sigma\left(T_s^4 - T_\infty^4\right)\right)A_s$$

Where $G_{measured}$ is the in-plane solar irradiation on the panel, calculated from the irradiation module. In addition, a radiative heat loss was included to account for the absorptivity of the ambient atmosphere and any cloud cover that might be present. This loss is also modeled with a grey body, where the temperature of the grey body is set to the ambient temperature minus 2 degrees Kelvin, and the emissivity of the gray body is dependent on the ambient relative humidity and cloud condition:

$$Q_{rad,loss} = \varepsilon(\%RH, \text{Cloud})\sigma A_s\left(T_s^4 - \left(T_\infty - 2\right)^4\right)$$

Where:

$$\varepsilon(\%RH, \text{Cloud}) = 1 - \left(\frac{\varepsilon_{\text{RH}} + \varepsilon_{Cloud}}{2}\right)$$

Where ε_{RH} and $\varepsilon_{\text{Cloud}}$ are the emissivity indices of the grey surface due to relative humidity and cloud cover, respectively:

Table 1: Relative Humidity Emissivity Indices

Relative Humidity (%)	Relative Humidity Index
RH < 65%	0
65%< RH < 70%	0.1
70% < RH < 75%	0.25
75% < RH < 80%	0.4
80% < RH < 85%	0.5
85% < RH	0.8

Table 2: Cloud Condition Emissivity Indices

Cloud Condition	Cloud Condition Index
Clear	0
Few	0
Scattered	0.05
Broken	0.25
Overcast	0.65
Haze	0.8

This approach greatly simplifies the calculations needed to determine the temperature of the solar cell. Notice that as the cloud cover or relative humidity increases, the radiation loss decreases, representing the effects of atmospheric radiation absorption and re-radiation. This assumption was made since it was deemed unnecessary to develop a physics of weather simulation for the purpose of determining the temperature of the solar cell, since the variation in the performance of the cell over the temperature range considered is relatively small, however it is significant enough to be included.

1.1.2 Model Verification

The model was constructed to simulate the performance of a Solarex MSX-60 60W solar panel array. Model verification of the power module is carried out by comparing simulation results to power data obtained from a 3.85 kW solar array on the rooftop of the Engineering Laboratory Facility at the University of California, Irvine. The simulated irradiation and cell temperature were used as inputs to the power module, and the results were compared to the measured power data. The individual 60W panel was scaled up to 3.85 kW for comparison.

The combined model was validated against measured power, cell temperature, and irradiation data from a 3.85 kW solar panel array on the roof of the Engineering Laboratory Facility at the University of California, Irvine.

Figure 2: Model Verification (a) Power Module, (b) Irradiation Model, (c) Temperature Module

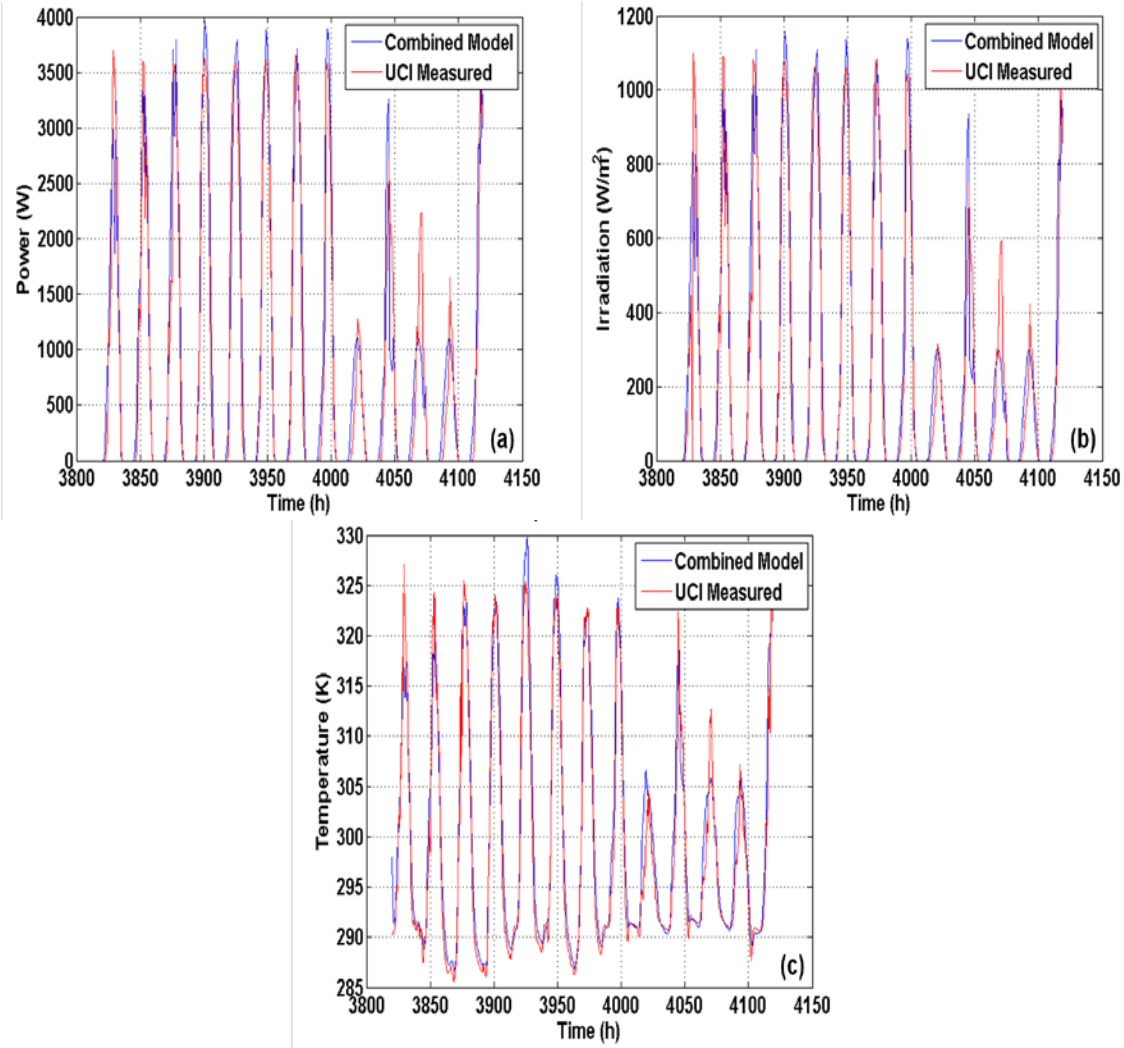

From Figure 2, the combined model results match with the measured data with an average error of 1.36% on a power output basis. Therefore, it is safe to assume that a more detailed model for determining the effective irradiation, power output, or cell temperature is not necessary for this level of analysis.

1.2 Lead-Acid Battery Model

1.2.1 Model Description

A lead-acid battery dynamic model based on equivalent circuit is developed. The model is designed to accept inputs for current and ambient temperature, and the outputs are battery voltage, state of charge (SOC) and battery electrolyte temperature. The equivalent circuit network represented in Figure 3 constitutes the basis on which the battery model developed in this report[7]. There were mainly three sub models: charge and capacity sub model, thermal

[7] M. Ceraolo, **New Dynamical Modeis of Lead-Acid Batteries**. IEEE Transactions on Power Systems, 2000. 15(4): p. 1184-1190.

(electrolyte heating) sub model and circuit network sub model. The model developed had been demonstrated to have accuracy satisfactory for majority of uses[8]. The dynamic model developed can be used for 1) simulate battery behavior under different operating conditions (both charge and discharge processes), 2) state of charge estimation, battery monitoring and diagnostics when lead acid battery is contained in on-line systems.

The temperature of battery is modeled by the energy balance equations. In the battery operation, the heat generation is ascribed to the ohmic heating by the sum of the energy charged and discharged from the battery (I^2R). The heat dissipation is modeled by free convection and radiation processes described in the Equation below. The convection coefficient (h) is evaluated based on empirical correlation of external free convection flows and Nusselt number.

$$Heat\ loss = q_{conv} + q_{rad} = h\pi D(T_s - T_{ambient}) + \varepsilon\pi D\sigma\left(T_s^4 - T_{ambient}^4\right)$$

Figure 3: Lead-Acid Battery Equivalent Circuit

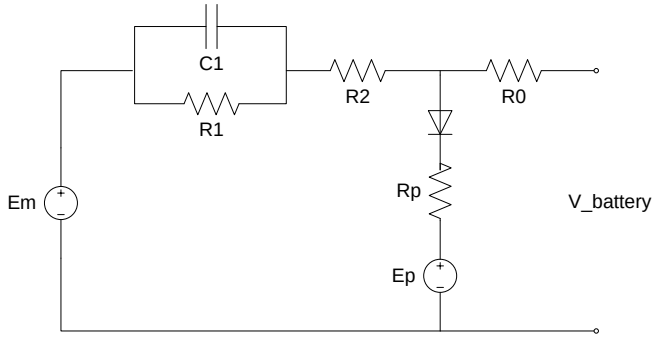

1.2.2 Model Verification

Model parameters were determined starting from sets of lab tests of real lead-acid batteries and empirical parameters used in literature models[9]. The parameter identification was simplified since some of the parameters can be taken as constant for all the batteries built with the same technology. The model was validated in conjunction with identifying the model parameters under various operating conditions.

The simulated battery behaviors agreed well with the experiment data in the literature of footnotes 7, 8 and 9. Some representative simulation results of a 2V 250Ah Lead-acid battery are shown in Figure 4, Figure 5, and Figure 6. Discharge (from fully charged) processes under

[8]M. Chen and G.A. Rincon-Mora, **Accurate Electrical Battery Model Capable of Predicting, Runtime and I-V Performance.** IEEE Transactions on Energy Conversion, 2006. 21(2): p. 504-511.

[9]S. Barsali and M. Ceraolo, **Dynamical Models of Lead-Acid Batteries: Implementation Issues.** IEEE Transactions on Energy Conversion, 2002. 17(1): p. 16-23.

various constant discharging currents (25A, 50A, 125A, 200A and 250A) starting are shown in Figure 4. The temperature effect on discharging is presented in Figure 5, in which a fully charge battery being discharged at current of 125A under various ambient temperatures.

Figure 6 presents the simulation of transient behaviors of the battery discharging under constant currents (0.2C for 2 hours and 4 hours) followed by rest periods (in which the current is zero) at 20°C.

Figure 4: Discharge under Constant Current, 20°C

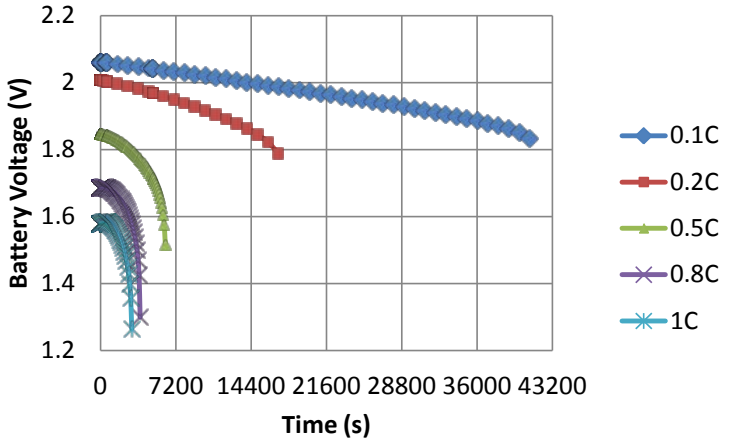

Figure 5: Discharge under 0.5C at Various Ambient Temperatures

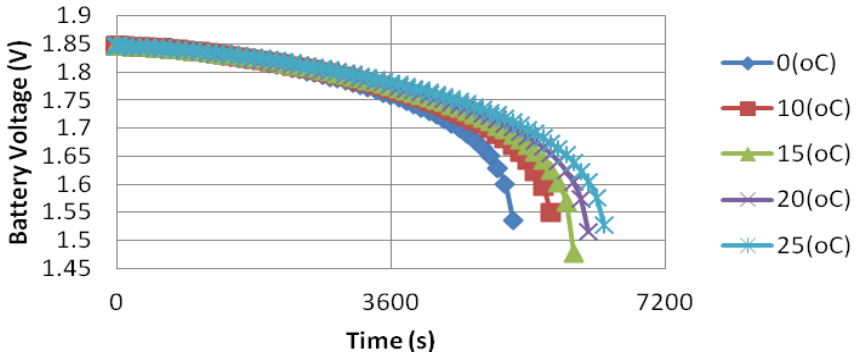

Figure 6: Discharge under 0.2C Current Step at 20°C

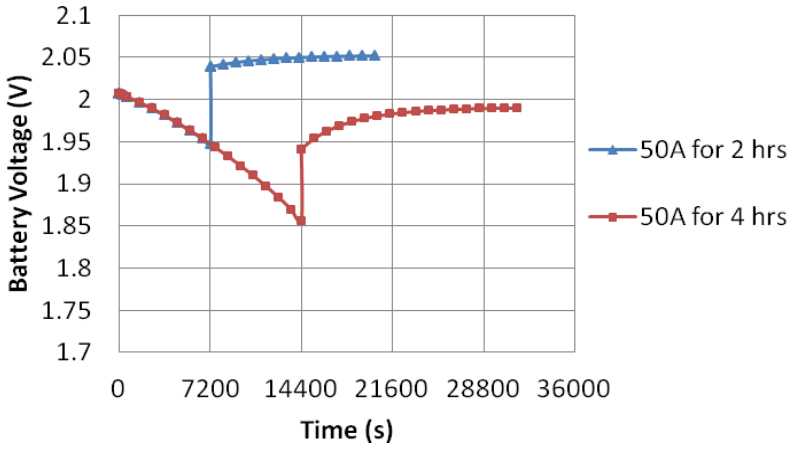

1.3 Lithium-Ion Battery Model

1.3.1 Model Description

A generic Lithium-ion battery dynamic model is developed and validated with a 3.3V 2.3Ah Lithium-ion battery (ANR26650M1, A123Systems®) based on a model proposed in[10] and the implemented battery model in SimPowerSystems™ in MATLAB/Simulink®. The model is using SOC as input and battery voltage as output, and simulated using a simple controlled voltage source in series with a constant resistance. The equivalent circuit of the non-linear battery model proposed in[10] is showed in Figure 7 and the parameters are listed in Table 3. Based on the discharge characteristics, all the parameters of the equivalent circuit can be modified to represent a particular battery type.

Figure 7: Non-Linear Battery Model

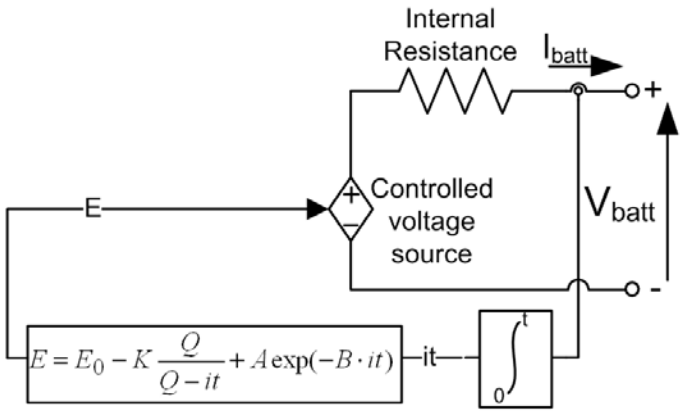

[10]Tremblay, O., L.A. Dessaint, and A.I. Dekkiche.**A Generic Battery Model for the Dynamic Simulation of Hybrid Electric Vehicles**. in Vehicle Power and Propulsion Conference, 2007. VPPC 2007. IEEE. 2007.

Table 3: Battery Model Parameters

E (V)	No load voltage
E_0(V)	Battery constant voltage
Q (A*h*)	Battery capacity
R(Ω)	Internal resistance
K(V)	Polarization voltage
A(V)	Exponential zone amplitude
B(A*h*)$^{-1}$	Exponential zone time constant inverse

The model developed is based on specific assumptions: 1) the internal resistance is assumed constant during the charge and the discharge cycles and does not vary with the amplitude of the current, 2) the parameters of the model are extracted from discharge characteristics and assumed to be the same for charging, 3) the capacity of the battery doesn't change with the amplitude of current, 4) the temperature doesn't affect the model's behavior, and the battery model is simulated the battery behavior at 25^{o}C. 5) the Self-Discharge of the battery is not simulated, and 6) the battery has no memory effect.

1.3.2 Model Verification

A series of voltage response experiment results for a higher power rechargeable Lithium-ion (ANR26550M1) battery under various constant discharging current were obtained from A123systems® and presented in Figure 8 and Figure 9. Fully charged batteries (SOC=100%) are discharged under 0.43C, and 4.35C, respectively.

According to Figure 8, which compares manufacture experimental results and our simulated voltage responses relative to complete discharges at 1A, the model developed accurately simulated the discharging processes starting from full charge (SOC=100%) to nominal voltage (3.3V). While from nominal voltage to recommended cut off voltage (2V), the simulation results are not agreed very well with the manufacture's data.

With increased discharge current to 4.35C (10A) presented in Figure 9, the simulation result agreed well with the manufacture data at the exponential zone where the beginning of the discharge, and power output is slightly larger from 3.2 V to cut off voltage.

Figure 8: Discharge Characteristics at 25°C, 1A

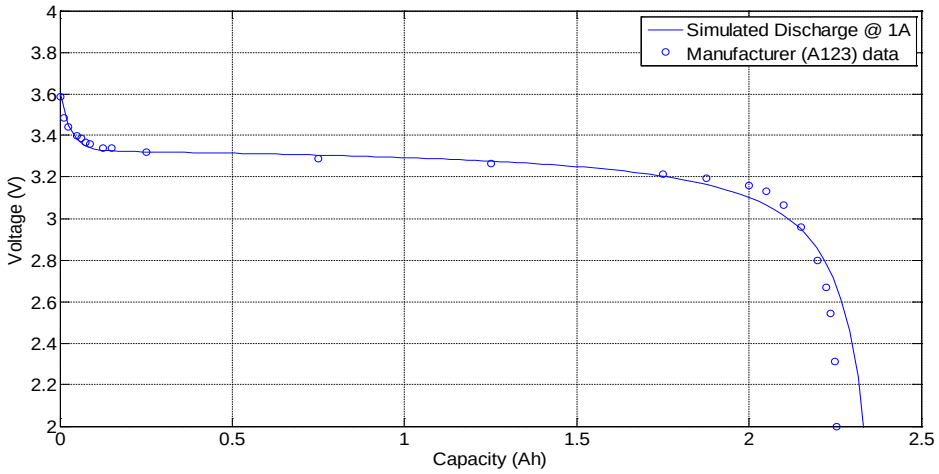

Figure 9: Discharge Characteristics at 25°C, 10A

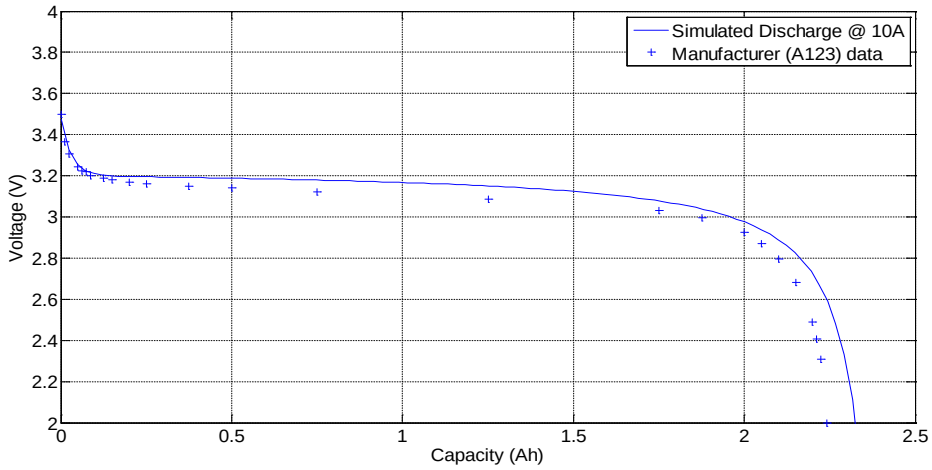

1.4 Ultracapacitor Model

Ultracapacitors or electric double layer capacitors (EDLC) are electrical energy storage devices which have significantly larger energy density as compared to common capacitors, and larger power density compared to conventional batteries. Ultracapacitors present the lowest cost per Farad, extremely high cycling capability and long shelf life (when using carbon electrode), and are environmentally safe[11]. Because of these unique characteristics, ultracapacitors are utilized in a wide range of applications, such as electric vehicles and distributed generation systems. The feature of larger energy density is mainly due to the enormous surface area created by the

[11]Burke, A., **Ultracapacitors: Why, How, and Where is the Technology**. Journal of Power Sources, 2000. 91(1): p. 37-50.

porous (carbon) electrodes and the small charge separation created by the dielectric separator in ultracapacitors[11].

1.4.1 Model Description

Dynamic modeling and simulation of ultracapacitors are very important for evaluating and understanding the ultracapacitor behavior under different operating conditions in various applications. The most commonly used model of ultracapacitor is the classical RC equivalent circuit model, which consists of a capacitance (C), an equivalent series resistance (ESR) representing the charging and discharging resistance, and an equivalent parallel resistance (EPR) that accounts for the self-discharging losses[12] [13]. In spite of being useful for many applications, this simple resistor and capacitor network model is insufficient to describe accurately the dynamics of an ultracapacitor[14]. Because of the porous nature of the ultracapacitor electrodes, the capacitive interface is not localized in a plain area but spreads into the inner of the highly distributed pores. Hence, the theoretical model was then developed to be a highly distributed R-C network which composed of many nonlinear resistors and capacitor leading to different time constants.

In this project, a dynamic ultracapacitor model based on a new equivalent circuit is developed and the model can predict the dynamic response of several types of ultracapacitors having different capacity and rated voltage values under various operating conditions. Further, an ultracapacitor bank built by arranging single ultracapcacitors in series is also developed and verified. Dynamic simulations are performed in MATLAB/Simulink® environment with Simpowersystem toolbox, and the simulations results were compared to the data provided by ultracapacitor manufacturer (Maxwell®).

The equivalent ultracapacitor circuit used in the model is shown in Figure. The single resistor of R1 represents the terminal interconnects resistance. While the resistor ESR represents the equivalent series resistance of the combined effect of interconnects, metal foil current collectors and interfacial resistance of carbon electrodes. Compared to the traditional RC network, the Cauer I network used in this study gives more insight into the origins of the three time constant approximation of an ultracapacitor model[15]. The branch of ESR-C_f, R_{d1}-C_{d1}, and R_{d2}-C_{d2} account for the highly distributed effects of carbon matte resistance, ionic conduction, and Helmholtz double layer capacitances existing at “macro”, “meso” and “micro” pores in the electrodes,

---

[12]Uzunoglu, M. and M.S. Alam, **Dynamic Modeling, Design and Simulation of PEM Fuel Cell/Ultra-Capacitor Hybrid System For Vehicular Applications**. Energy Conversion and Management, 2007. 48(5): p. 1544-1553.

[13]Vural, B., et al. **A dynamic Ultra-Capacitor Model For Vehicular Applications**. in Clean Electrical Power, 2009 International Conference on. 2009.

[14]Belhachemi, F., S. Rael, and B. Davat. **A Physical Based Model of Power Electric Double-Layer Supercapacitors.**in Industry Applications Conference, 2000. Conference Record of the 2000 IEEE. 2000.

[15]Miller, J.M., P.J. McCleer, and M. Cohen, **Ultracapacitors as Energy Buffers in a Multiple Zone Electrical Distribution System**, Maxwell Technologies, Inc.

respectively[15]. The resistor R_{leak} represents the self-discharge behavior of ultracapacitor, and which is important factor to determine the duration time of stored energy at open circuit.

Figure 10: Equivalent Circuit Model of Ultracapacitor

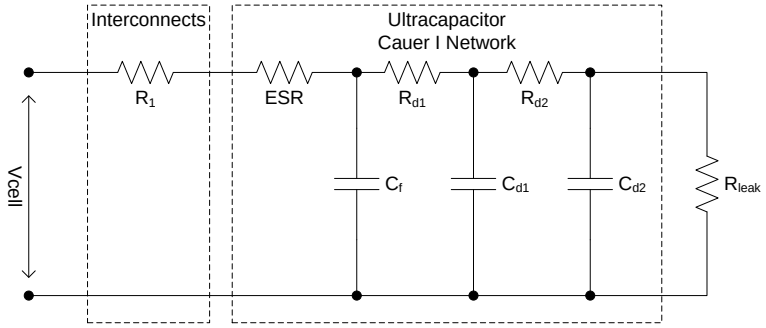

1.4.2 Model Verification

In this project, MATLAB/Simulink® is used to develop the dynamic ultracapacitor model. To test the developed dynamic model, various charge/discharge conditions are used in DC regime. The extraction of model parameters is achieved by comparing the simulation results and the data provided by Maxwell®. In this section, a Maxwell® 2000 F ultracapacitor (BCAP2000-P270, rated as 2000F, 2.7V) is first simulated and verified. By varying model parameters with the same equivalent circuit, a Maxwell® 3000F ultracapacitor (BCAP3000-P270, rated as 3000F, 2.7V) is then simulated and verified. Further, to simulate an ultracapacitor bank, a Maxwell® 16V ultracapacitor module (BMOD0500-P016) is simulated and verified. Three types of ultracapacitors and their rated voltages and capacitances are listed in Table 4.

Table 4: Commercial (Maxwell®) Ultracapacitors Simulated

Ultracapacitor	Capacitance (F)	Rated Voltage (V)	Rated ESR (mΩ)
BCAP2000-P270	2000	2.7	0.35
BCAP3000-P270	3000	2.7	0.29
BMOD0500-P016	500	16.2	2.4

1.4.2.1 Single Ultracapacitor Rated at 2000F, 2.7V

Constant current tests represent a basic and a widely used characterization method that is useful to determine the rated capacitance and the equivalent series resistance (ESR)[16]. A series of voltage response experiment results for BCAP2000-P270 under various constant discharging

[16]Lajnef, W., et al., **Characterization Methods and Modelling of Ultracapacitors For Use as Peak Power Sources**. Journal of Power Sources, 2007. 168(2): p. 553-560.

current was obtained from Maxwell® and presented in Figure 11. According to Figure 11, which compares Maxwell® experimental results and our simulated voltage responses relative to complete discharges at various constant currents, the model developed accurately simulated the discharging processes starting from full charge. In Figure 12, voltage response results when discharging the ultracapacitor with constant power provided by Maxwell® and our simulation results were presented, and it can be seen that the results obtained by the simulation are in good agreement with the experimental results of Maxwell® for BCAP2000-P270 in the range of 1.35V-2.7V at various constant power. For capacitance and ESR characterization of ultracapacitor products, Maxwell® uses a constant current test method called 6-step process. In terms of BACP2000-P270 ultracapacitor, a test including charge device to rated voltage at 250 A, rest, discharge device to one-half its rated voltage at 250 A, rest, and end test after discharge to a low safe voltage (<0.1V). Maxwell® provided the experiment results and simulation results obtained using their model which are shown in Figure 13. The simulation result obtained by the model developed in this study was also showed in Figure 13, which is also in good agreement with the experiment data. Figure 13 also indicate that the model developed by Maxwell® is more accurate than the one developed in this study in terms of the dynamic response at 250A discharging rate. The model developed in this project is more accurate when discharging occurs at lower current (≤200A). The parameter values for BCAP2000-P270 model are listed in Table 5.

Figure 11: Simulation and Experimental Results for a 2000F Ultracapacitor (Maxwell® BCAP2000-P270) Discharging at Various Constant Current

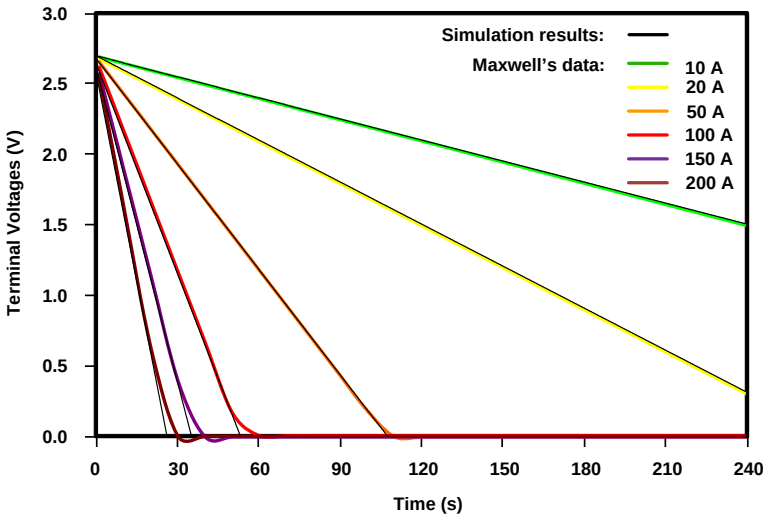

Figure 12: Simulation and Experimental Results for a 2000F Ultracapacitor (Maxwell® BCAP2000-P270) Discharging at Various Constant Power

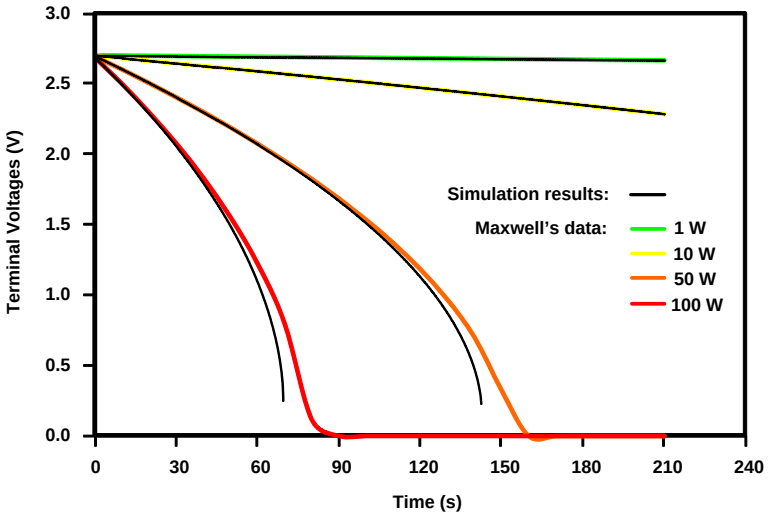

Figure 13: Simulation and Experimental Voltage Response Results for a 2000F Ultracapacitor (Maxwell® BCAP2000-P270) under 6-step Test Procedure

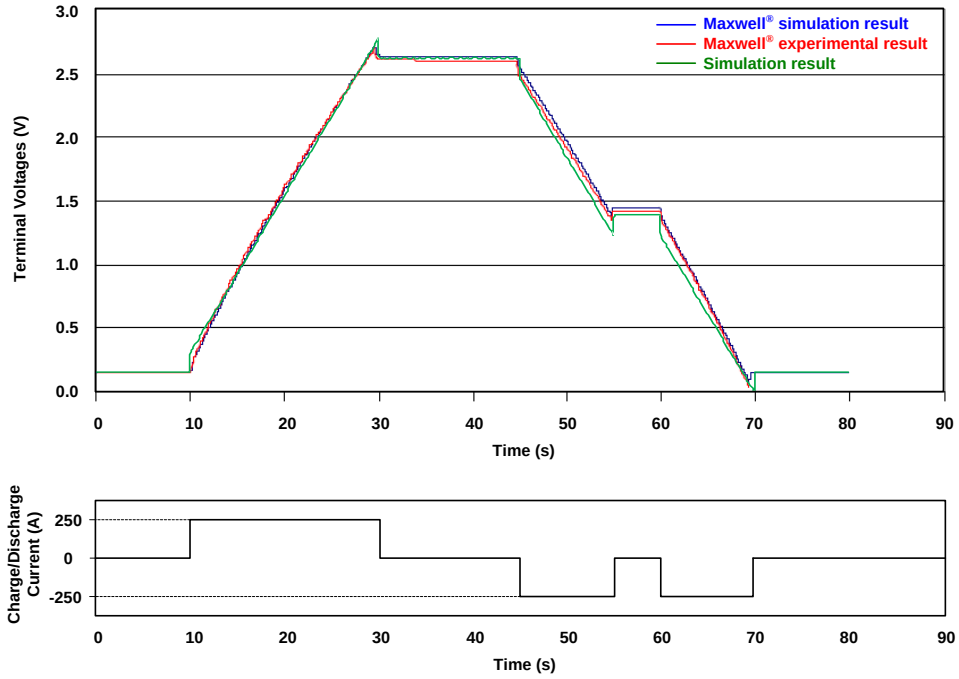

1.4.2.2 Single Ultracapacitor Rated at 3000F, 2.7V

By varying model parameters of the ultracapacitor model developed, Maxwell® BCAP3000-P270 was simulated and the simulation results were compared to the manufacture data and presented in Figure 14 and Figure 15, and the parameter values for BCAP3000-P270 model are

listed in Table 5. As shown in Figure 14, the model developed accurately simulated the discharging processes starting from full charge under various discharging current. And it also can be seen that the discharging results obtained by the simulation are in good agreement with the experimental results in the range of 1.35V-2.7V at various constant power in Figure 15. The model developed in this project shows higher accuracy at lower constant power discharge rate.

Figure 14: Simulation and Experimental Results for a 3000F Ultracapacitor (Maxwell® BCAP3000-P270) Discharging at Various Constant Current

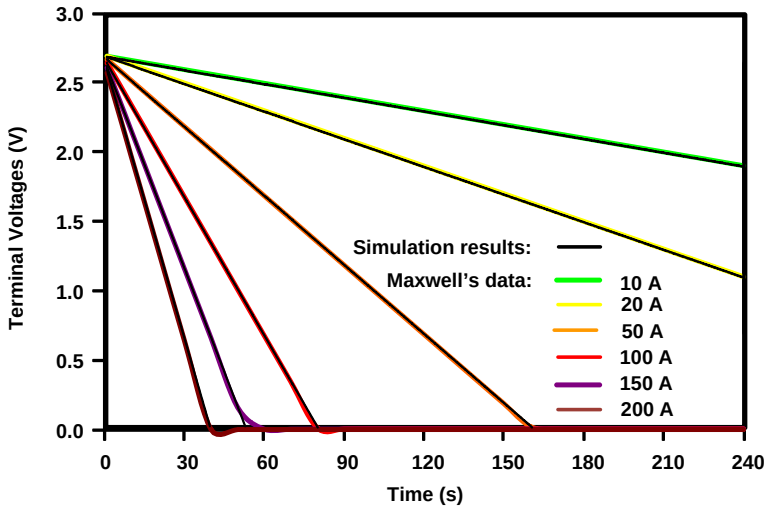

Figure 15: Simulation and Experimental Results for a 3000F Ultracapacitor (Maxwell® BCAP3000-P270) Discharging at Various Constant Power

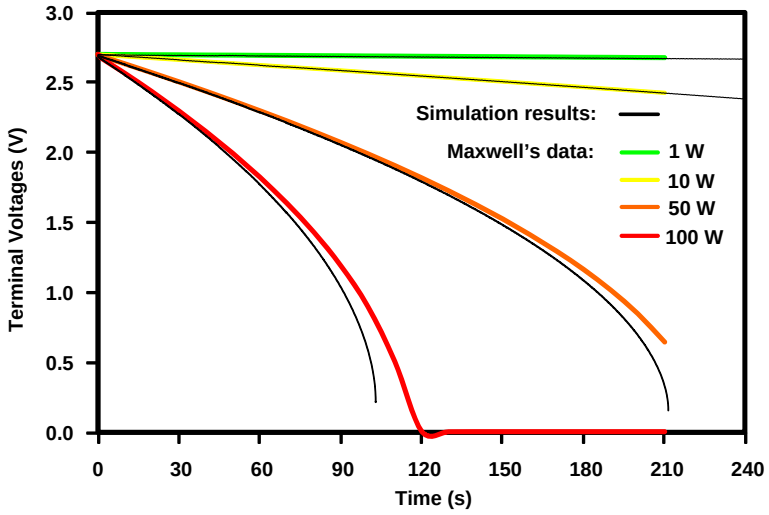

Table 5: Model Parameters for BCAP2000 and BCAP3000 Ultracapacitor

Parameters	BCAP2000 MODEL	BACP3000 MODEL
R_1	0.213 mΩ	0.18 mΩ
ESR	0.35 mΩ	0.29 mΩ
R_{d1}	0.142 mΩ	0.12 mΩ
R_{d2}	0.355 mΩ	0.3 mΩ
C_f	800 F	1200 F
C_{d1}	880 F	1320 F
C_{d2}	320 F	480 F
R_{leak}	675 Ω	675 Ω

1.4.2.3 Ultracapacitor Bank Rated at 500F, 16.2V

In practical applications, the certain amount of terminal voltage and energy or the capacitance of ultracapacitor storage system can be achieved by stacking multiple ultracapacitors in series and/or parallel. The terminal voltage required determines the number of capacitors that must be connected in series to form a bank and the total capacitance the total equivalent circuit resistance can be calculated as:

$$C_{total} = N_p \cdot \frac{C}{N_s}$$

$$R_{total} = N_s \cdot \frac{ESR}{N_p}$$

Where N_s is the number of ultracapacitors connected in series, N_p is the number so series strings in parallel, C is the capacitance for single ultracapacitor, ESR is equivalent series resistance for single ultracapacitor, C_{total} is the total system capacitance, and R_{total} is the total system resistance. By calculation, the Maxwell® BMOD0500-P016 is made up of 6 Maxwell® BCAP3000-P270 in series in terms of rated operating voltage and capacitance.

After the single ultracapacitor (BCAP3000-P270) is simulated and verified, a 16.2 V ultracapacitor bank model is developed by connecting 6 single ultracapacitor equivalent circuit models in series. The simulation results are compared to manufacturer's data and showed in Figure 16 and Figure 17.

Depending on the physical structure nature, the maximum voltage that can be applied across a single ultracapacitor is limited, typically 2.5~2.7V. Exceeding of this voltage will lead to a reduction of the lifetime or even catastrophic failure. As a consequence of this limitation, many of such cells have to be connected in series for applications required higher operating voltage, especially in automotive and residential uses. When connecting many ultracapacitors in series, a disadvantage of this high voltage ultracapacitor series module is the asymmetrical balance of the voltage. If there is difference in the values of each ultracapacitor in series, the total voltage over the series connection will not be equally distributed between the different ultracapacitor which resulted in asymmetrical voltage distribution. With increasing charge/discharge cycles, a

local over-voltage could appear over one of several ultracapacitors and decrease the lifetime. Ultracapacitor series model developed in this study assumed that component as ideal ultracapacitors with identical capacitance and leakage current, thus voltage balancing would not be an issue. In terms of operation, there are several ways to balance the ultracapacitor series module, such as passive voltage balancing and active voltage balancing. A limitation of the model developed is that the temperature is not consider and assumed all ultracapacitors working at room temperature (25°C).

Figure 16: Simulation and Experimental Results for a 500F Ultracapacitor (Maxwell® BMOD0500-P016) Discharging at Various Constant Current

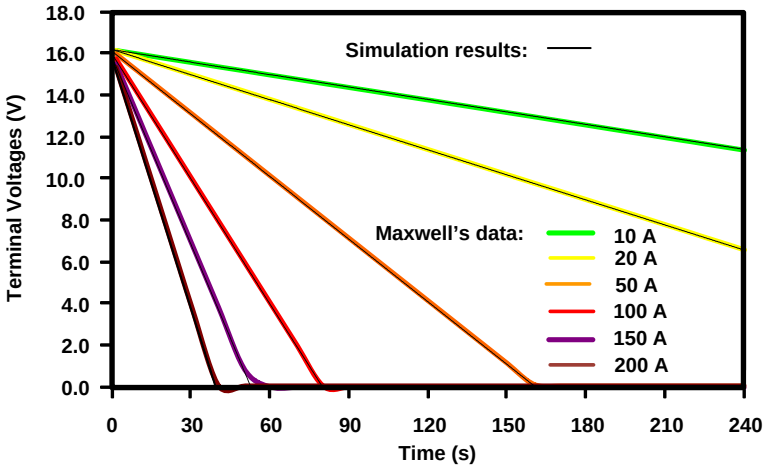

Figure 17: Simulation and Experimental Results for a 500F Ultracapacitor (Maxwell® BMOD0500-P016) Discharging at Various Constant Power

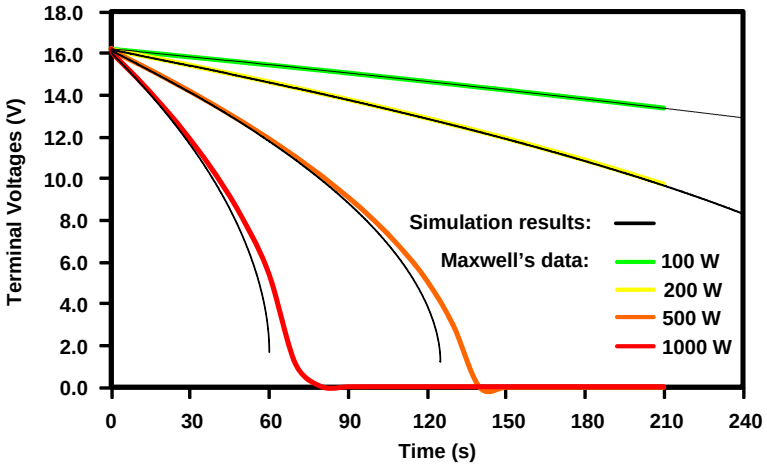

1.5 Heat Recovery Steam Generator Model

1.5.1 Model Description

The Heat Recovery Steam Generator (HRSG) system was modeled with classical approaches to estimating heat exchanger effectiveness. The primary means of estimating heat transfer for the complex geometries involved in the HRSG was the ε–NTU Method. This method assumes a heat exchanger effectiveness as follows:

$$\varepsilon = \frac{q}{q_{\max}} \qquad 0 \le \varepsilon \le 1$$

For this method, the maximum heat transfer rate is given by the following expressions

$$q_{\max} = C_{\min}\left(T_{h,i} - T_{c,i}\right)$$

$$C_{\min} = \begin{cases} C_h \text{ if } C_h < C_c \\ \text{or} \\ C_c \text{ if } C_c < C_h \end{cases}$$

where $C_i = m_i c_{P,i}$ or thermal flow rate

where q_{max} depends upon the limiting thermal flow rate, and c_P is evaluated at the mean temperature of the heat exchanger. The number of transfer units, NTU, an important parameter in the current analysis, is given by

$$NTU \equiv \frac{UA}{C_{\min}}$$

The definition of heat transfer for any heat exchanger is provided by the following equation:

$$q \equiv UA\Delta T_{mean} \quad \text{where } \Delta T_{mean} \text{ is mean temperature difference}$$

For a counter-flow heat exchanger the log-mean temperature difference (LMTD) is given by the following:

$$\Delta T_{mean} = \text{LMTD} \quad = \frac{\Delta T_1 - \Delta T_2}{\ln\left(\Delta T_1 / \Delta T_2\right)}$$

Based upon the effectiveness definition, the heat flux in the HRSG components can be calculated as follows

$$q = \varepsilon C_{\min}\left(T_{h,i} - T_{c,i}\right) = C_h\left(T_{h,i} - T_{h,o}\right) = C_c\left(T_{c,o} - T_{c,i}\right)$$

where the effectiveness in terms of dimensionless parameters is provided as

$$\varepsilon = f\left(NTU, C_r\right) \quad \text{where } C_r = C_{\min}/C_{\max}$$

When there is a phase change, as there is when water is being boiled in the steam drum of the HRSG then phase change must be accounted for as follows

$$\varepsilon = f\left(NTU\right) \quad \text{because } C_r \to 0$$

Given the equations presented above, the modeling solution methodology contains the following steps:

1. Find the Effectiveness for the HX with cross-flow configuration
2. Knowns
    a. Temperatures of cold side, $T_{c,I}$ and $T_{c,o}$
    b. Outlet temperature of hot side $T_{h,o}$
    c. Correction factor to LMTD for cross-flow
3. Unknowns
    a. Inlet temperature of hot side $T_{h,i}$
4. Assumptions
    a. Cp values based on average temperatures, no heat loss to surroundings, no thermal resistance from tube wall, fully-developed flow, internal losses accounted for by effectiveness
5. Determine the effectiveness
    a. Effectiveness look-up table

Figure 1 presents the steps in the solution strategy for calculating heat exchange in a heat exchanger with cross-flow configuration. Note that the solution requires a multi-variable regression step, which requires an iterative solution. This regression analysis was checked and found to accurately produce effectiveness values as shown in Figure 19.

Figure 18: Steps in Solution Strategy for Heat Exchange in the Cross-Flow Configuration

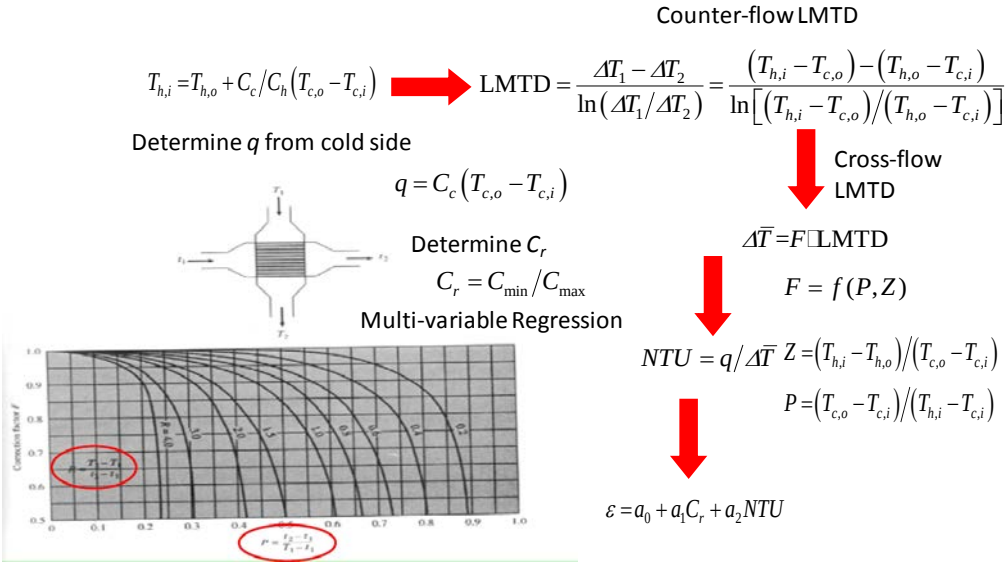

Figure 19: Accuracy Check of the Regression Analysis for ε

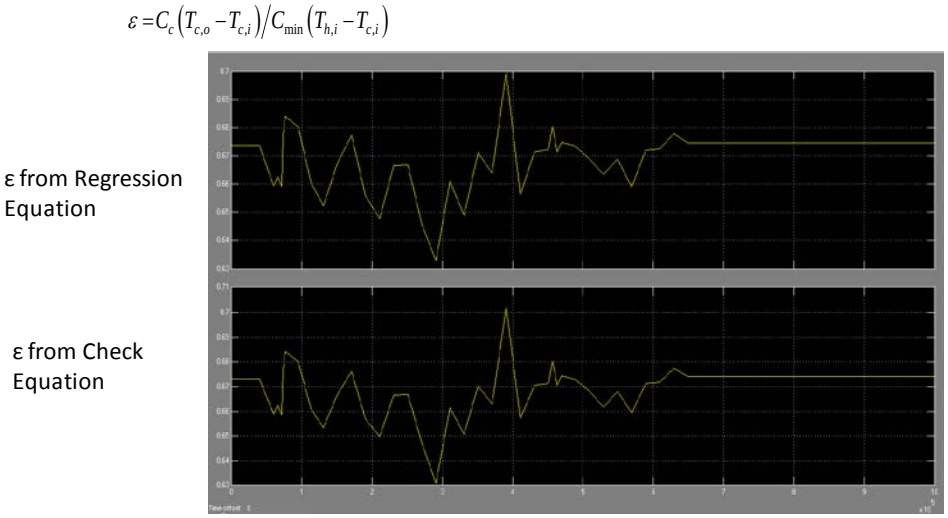

1.5.2 Model Verification

After producing this HRSG model, comparisons to data from the HRSG were accomplished. Figure 20 presents a comparison of HRSG simulation results with 3-weeks of data from the UCI Central Plant HRSG, showing a reasonably good comparison for the hot temperature in.

Figure 20: Comparison of HRSG Simulation Result with 3-Weeks of Data from the UCI Central Plant HRSG

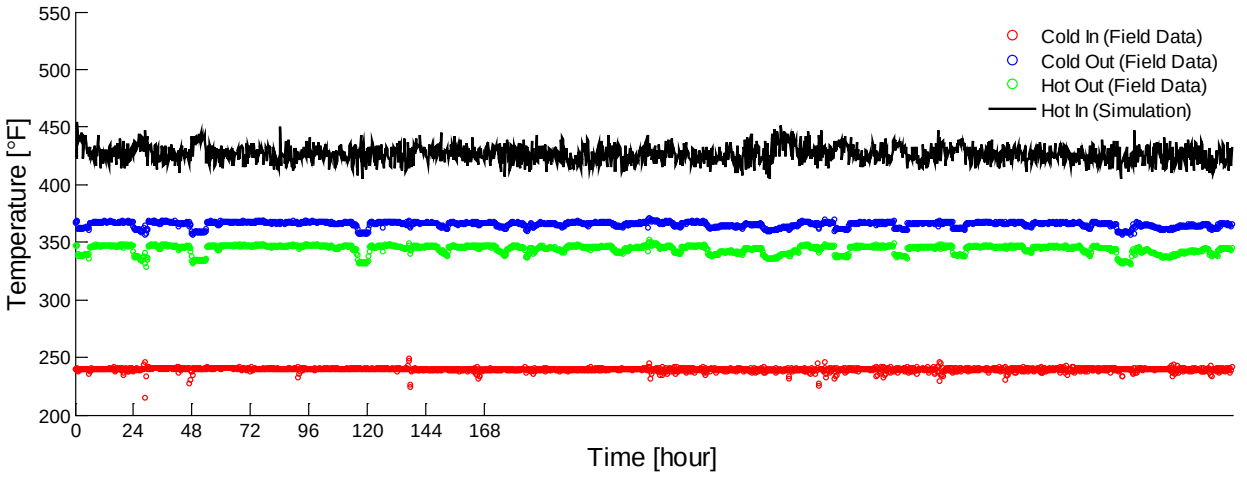

A second comparison was made for model verification in which only the cold side temperature is assumed to be known and in which a constant NTU was assumed. Results from this comparison are presented in Figure 21.

Figure 21: Comparison between HRSG Model and Data for the Case When Cold Side Temperature is Known

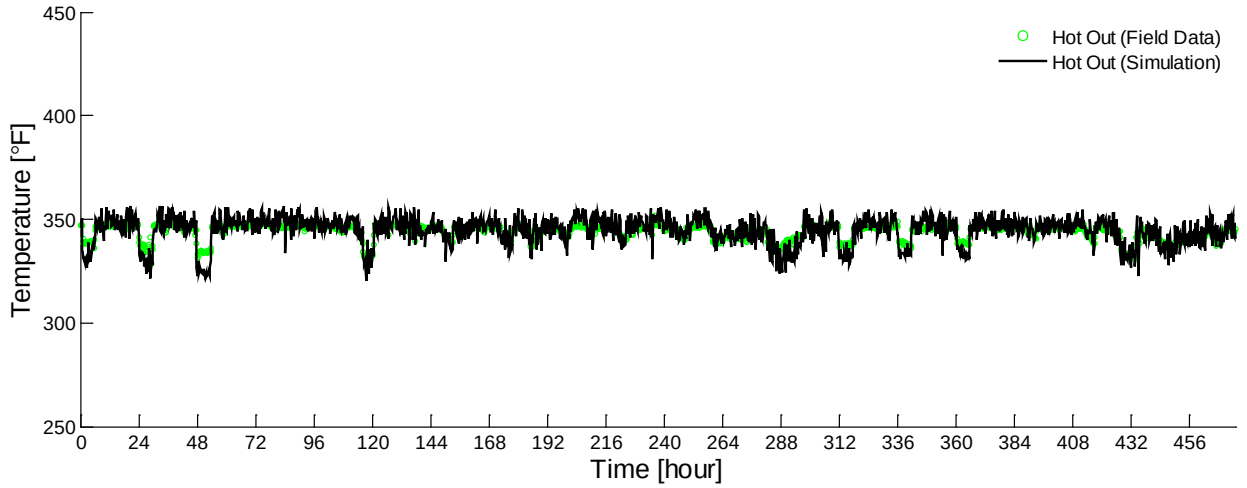

1.6 Steam Turbine Model

1.6.1 Model Description

The physical dynamic model of the steam turbine is based on first-principles thermodynamics and is developed and verified against in-field operation data. The mass balance for the steam turbine is given as

$$V_{cv}\frac{d\rho}{dt} = \dot{m}_{in} - \dot{m}_{out}$$

The transient energy balance takes into account the enthalpy difference between the inlet and outlet steams, the work done on the turbine blades by the steam, and a constant heat loss to the surrounding. The governing equation for the energy balance is thus,

$$\rho C_p V_{cv}\frac{dT}{dt} = \dot{m}h\big|_{in} - \dot{m}h\big|_{out} - \dot{W}_{st} - \dot{Q}_L$$

where $\dot{W}_{st}$, the actual mechanic work, deviates from the ideal mechanical work according to its isentropic efficiency and is given by the expression,

$$\dot{W}_{st} = \eta_{isen}\left(\dot{m}h\big|_{in} - \dot{m}h\big|_{out}\right)$$

All thermodynamic properties for steam are obtained from steam tables derived from IAPWS IF-97. Peak isentropic efficiency of 0.9 was used for the model, representing the typical value for steam turbines. Important design characteristics for the Central Plant turbine are synchronous generator, inlet-pressure valve control, operating pressure range 230 psig inlet and 15 psig outlet.

The off-design performance of the steam turbine was simulated using a steam turbine performance curve derived from part-load study as reported by Fallah (Fallah, 1978).

1.6.2 Model Verification

In this section, the accuracy and performance of the model is verified. The steady-state response of the model is simulated over the operational range of the steam turbine. For the steam turbine at UCI Central Plant the cut-in power output is 500 kW, which corresponds to about 10,000 pounds per hour (pph) of steam flow. The model simulates the steady-state response of the steam turbine over operational range between 500 kW to 5.5 MW. The model predicted generator load versus throttle flow is compared to the aggregated results of the actual generator load versus throttle flow of the steam turbine for July 1-7, 2010 of 15-min temporal resolution. The comparison provided in Figure 22 shows reasonable agreement between simulated results versus in-field data.

Figure 22: Simulated Results of Generator Power Versus Throttle Steam Flow to the Steam Turbine as Compared to in-Field Data for Summer Week, July 1-7th, 2010

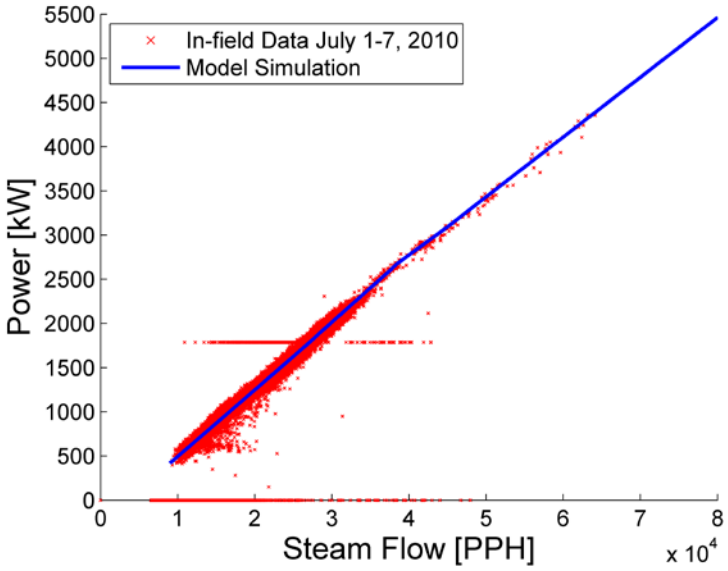

Note: high temporal data resolution was collected at 15-min intervals.

During transient operation, load change of the steam turbine is controlled by the inlet control valve or valves. These valves, of various types such as poppet, spool, or grid, can be operated by either a bar lift mechanism or a cam lift mechanism that is actuated based upon the operating steam pressure. For simplicity, the transient response of the steam turbine model employs the use of a first-order transfer function with a time constant of 1s to emulate the physical actuation of the valves. Figure 23 displays the recorded flow and pressure of the superheated steam from the HRSG section for the week of July 1-7, 2010. These transient parameters are input into the steam turbine model. The simulated generator output is provided in Figure 24 as compared to the actual generator output.

Figure 23: Operational Parameters Steam Flow and Inlet Pressure For July 1-7, 2010

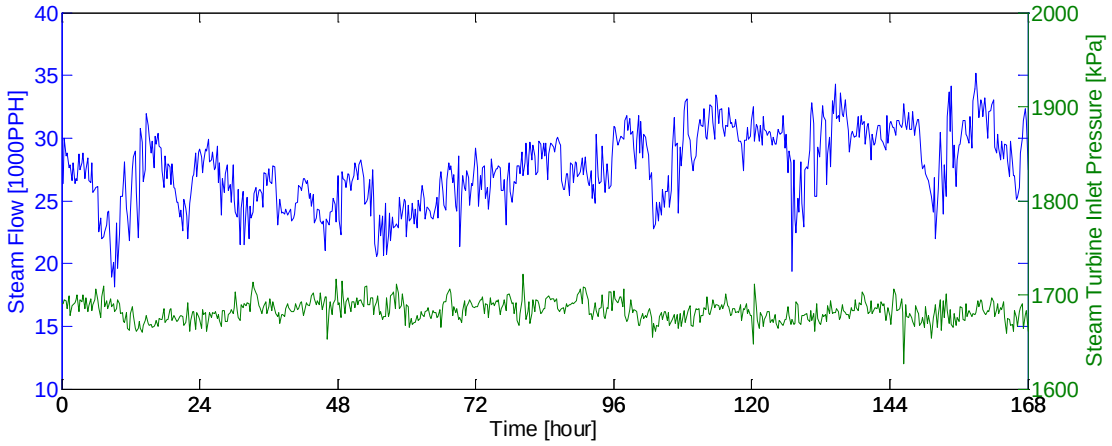

These parameters are the inputs into the steam turbine model

Figure 24: Transient Simulated Results Versus Transient Performance (15 Min) of the Actual Engine for the Week of July 1-7, 2010

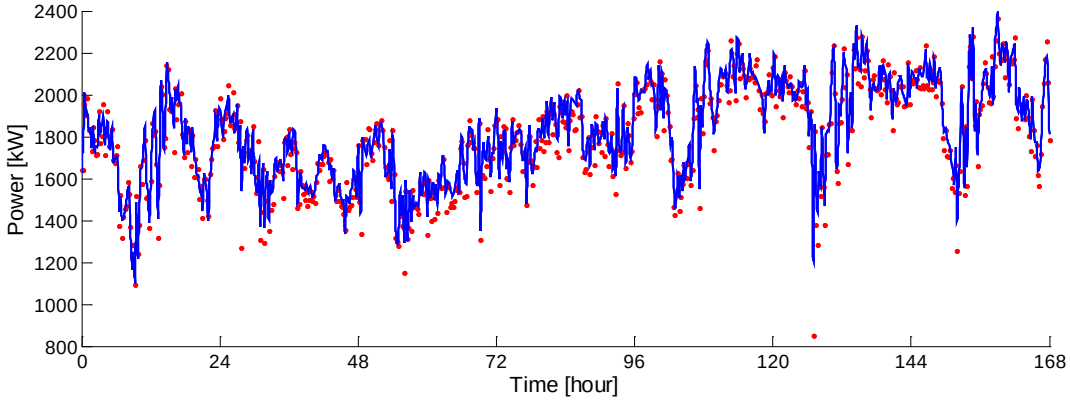

CHAPTER 2:
Building Dynamic Data Acquisition and Analysis

2.1 Engineering Laboratory Facility (ELF) Dynamic Data

To better characterize the ELF building's power demand profile, basic load analysis is carried out using descriptive statistic method. Electrical energy consumed and recorded every 15mins throughout the year of 2009 are translated to average power demand every 15mins. The data set is consists of 364 days and 96 data points in each day. The 15 minutes average power demand data of ELF are first visually depicted using box plot and five-number summaries: sample minimum, lower quartile, median, upper quartile and largest observation are presented. In Figure, the bottom and top of the box (in blue) are the 25th and 75th percentile (the lower and upper quartiles, respectively), and the band (in red) near the middle of the box is the 50th percentile (the median). The lower whisker represents the lowest datum that within 1.5 IQR (interquartile range) of the lower quartile, and the higher whisker represents the highest datum that within 1.5 IQR of the upper quartile. (+) denotes the outliers that are data with values beyond the ends of the whiskers. The spacing between the different parts of the box can indicate the degree of the dispersion of the data. The characteristics of the ELF building power demand are summarized below based on the results:

1. Only 9 weeks in 2009 did not have any outliers.
2. Throughout 2009, 75th percentile of daily power demand is in the range of 100kW to 120kW.
3. Throughout 2009, only 12 days have 75th percentile of daily power demand larger than 150kW.
4. Throughout 2009, the extreme daily load (lower whisker to upper whisker) is in the range of 20kW to 150kW.
5. Throughout 2009, the median daily load is in the range of 60kW to 90kW.
6. (demand charge issues) 17 days in 2009 have maximum power larger than 300kW as shown in the plot below:
7. (demand charge issues) 86 days in 2009 have maximum power larger than 200kW, as shown in the plot below:

The characteristics of the ELF building power demand are summarized below based on the results:

1. Most outliers > 300kW occur during 12pm to 6pm
2. 200kW power demand occurred during 6am to 6pm

The results indicate that the outlying power demand is likely associated with equipment that is operated during the day, most likely associated with the research purposes of the ELF building.

The results also indicate that the peak demand is not too much larger than the base demand of the building, which is most likely due to the fact that all of the building heating and cooling is provided by the central plant of UC Irvine.

Figure 25: Daily Boxplot of ELF Power Demand in 2009

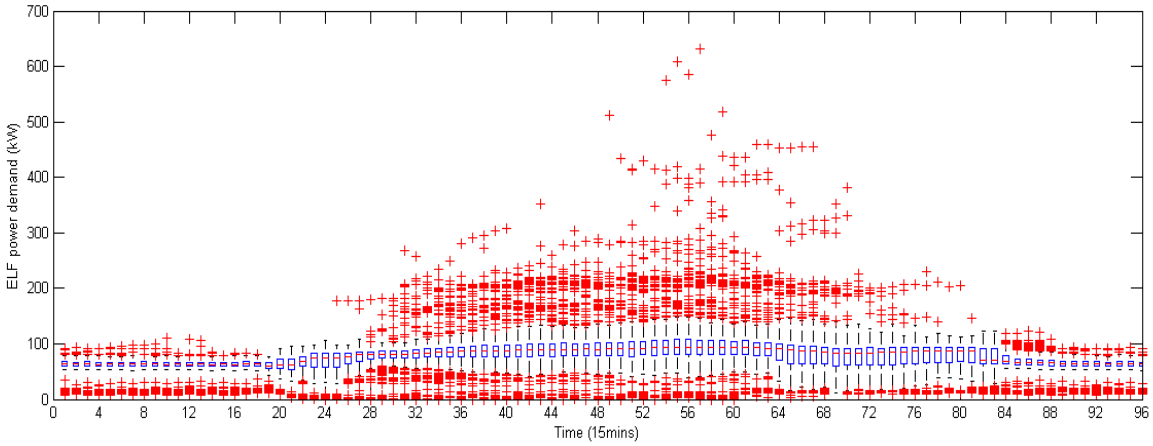

2.1.1 ELF Load Underlying Probability Distribution

The data set of ELF 15 minutes average power demand is then compared to a theoretical normal distribution in a probplot shown in Figure 26. As shown in the figure, in the range of 80kW to 110kW, the power demands follow a normal distribution well. Power demand larger than 210kW has a probability of ~1% throughout the year of 2009. These "irregular" loads are the main reason of demand charges.

Figure 26: Probability Plot of ELF Power Demand (per 15 minutes) in 2009 Compared With Normal Distribution

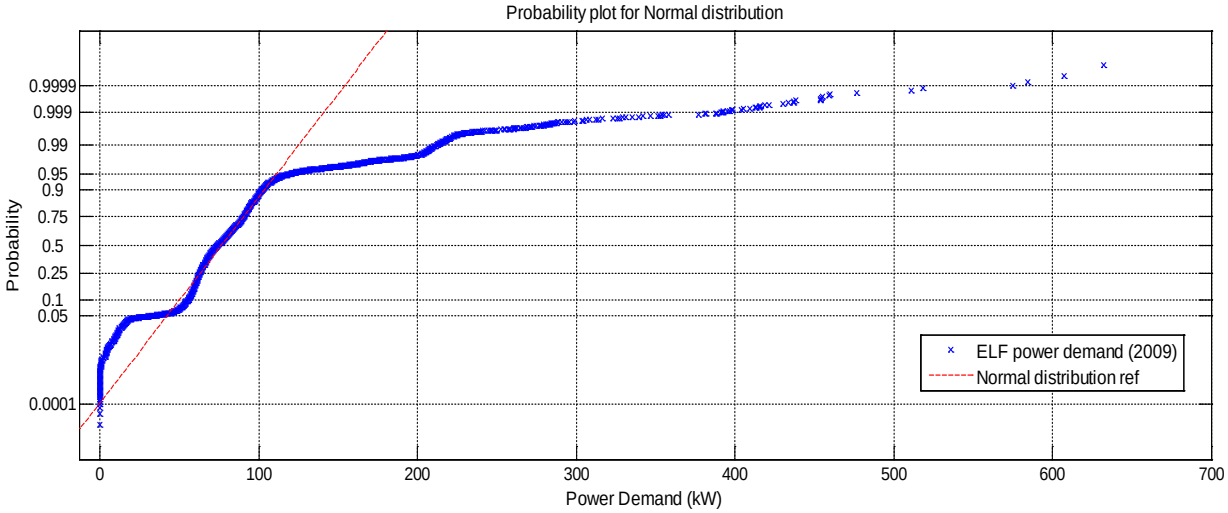

2.1.2 ELF Load Analysis

The electrical loads analysis of ELF building in 2009 is carried out and the characteristics of the building loads are described using Boxplot and Probplot. The results are important to size the battery/ultra-capacitor storage capacity and the distribution generation devices. In the next section the ELF model uses a PV generation of 60kW and a Li-ion battery bank of 45kWh capacity as power supplier other than the grid.

2.2 Engineering Laboratory Facility (ELF) Hybrid Energy Storage System Coupled to PV Generation

2.2.1 ELF Building Power Demand Profile

Energy consumption data (kWh) of Engineering Laboratory Facility (ELF) building in University of California, Irvine is acquired from iTron and provide by Chris Hartley. The range of the data is chosen as a summer week from August 2nd to 8th, 2009. The original data appeared to have 12 hour delay and has been adjusted accordingly to represent a typical summer week in southern California start from Sunday. The power profile of ELF building is showed in Figure 27.

Figure 27: ELF Building Power Demand Profile, Sunday August 02 to Saturday August 08, 2009

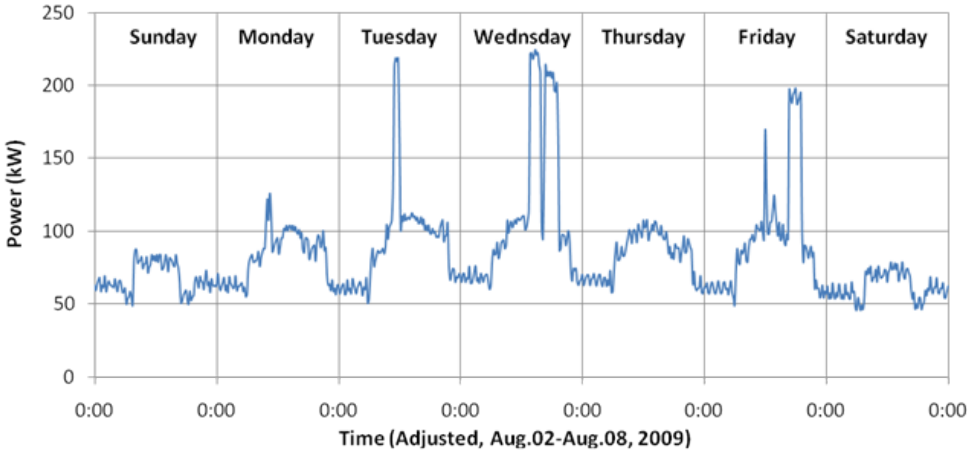

2.2.2 ELF Building Battery-Only System Configuration

Dynamic model of a hybrid PV-Grid power and Li-ion battery storage system has been developed and the system schematic is showed in Figure 28. In this, the size of PV system a nominal 60kW PV system based upon a previous APEP PV model is used in this model, the PV power supply profile is showed in Figure 29. 75kW constant power is supplied from the grid to meet the base load. Figure 30 shows the system net power profile, since this preliminary case use 75kW base load supply from grid, the access power (area above x-axis in Figure 30) is more than net power demand (area below x-axis in Figure 30). The based load power supply from grid will be further optimized. DC/AC inverter is currently simplified using conversion efficiency at 97%. And in the future a physical inverter model will be applied in the system.

The lithium-ion battery band used in this system is composed of 6000 A123 systems ANR26650m1 Li-ion battery (2.3Ah, 3.3V). The number and the way to connect batteries are not optimized. Currently, 10 parallel branches of 600 batteries in series are used. The residential hybrid system model recently developed showed that battery bank composed of 600 single batteries in series could fully provide the storage capacity. The cost of each ANR26650m1 cell is around $20, therefore the battery storage component in this preliminary study costs about $120k.

Figure 28: Battery Only System Schematic

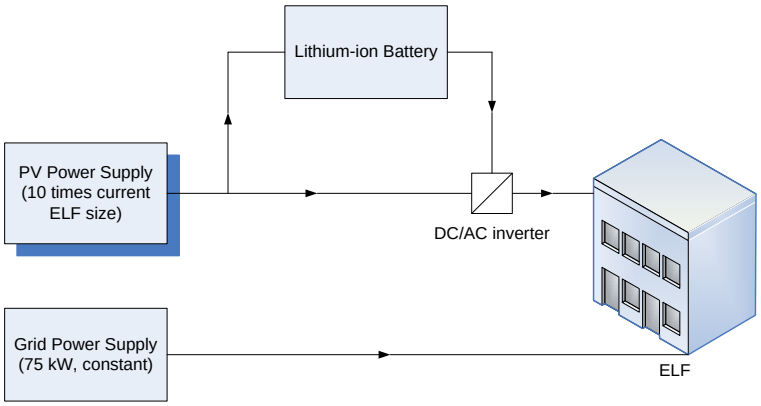

Figure 29: ELF Power Demand and PV Power Supply

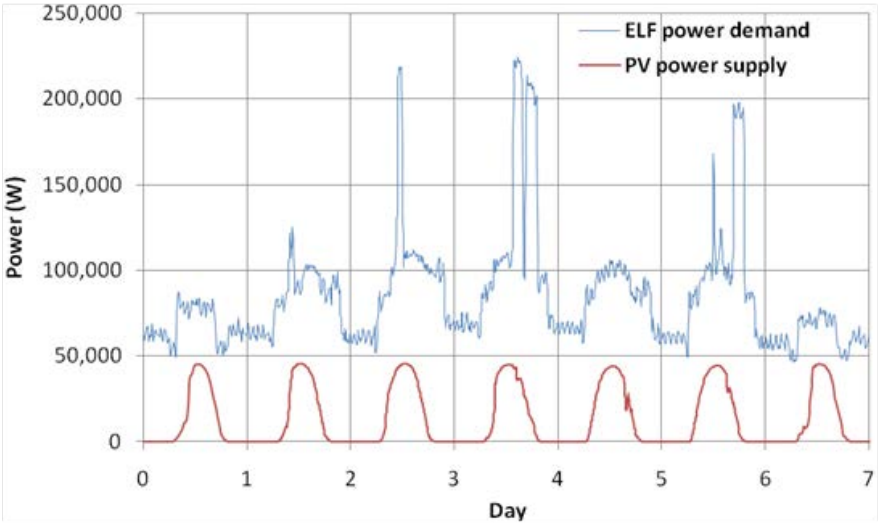

Figure 30: System Net Power Supply During the Week

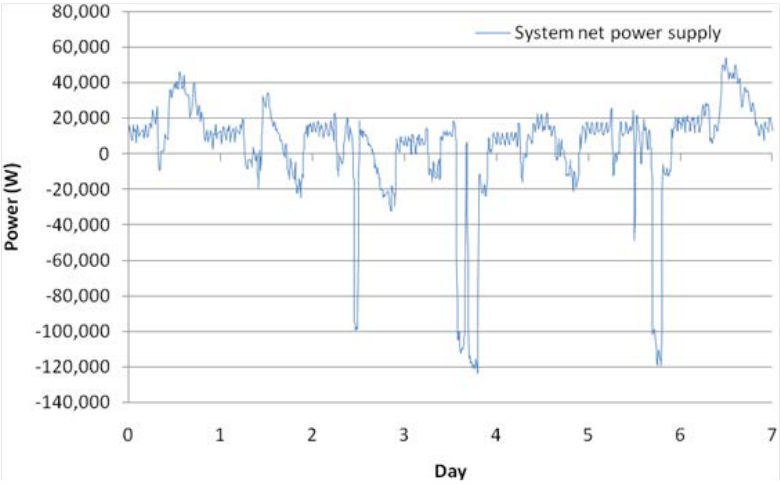

2.2.2.1 Control Strategy

The control strategy used in the current simulations possesses the following characteristics:

a. Constant 75kW power supply from utility grid.

b. PV power is always sent to meet building load demand.

c. If excess PV power is available then it is sent to the battery.

d. If PV power cannot meet the load demand, then use the energy stored in the battery.

e. Battery SOC=100% at t=0.

f. State of charge range = 95% to 20%.

2.2.3 Simulation Results

Battery current: The maximum fast charge/discharge current for ANR26650m1 battery is **10A**, and the simulation result in Figure 31 shows that during the peak load in noon, the maximum current in the battery is over 60A. In the future, current limitation of the battery will be added to the control strategies and the maximum current in the battery will be controlled within 10A, and the rest of the peak power demand will be supplied by ultra-capacitor.

Figure 31: Battery Current During the Week

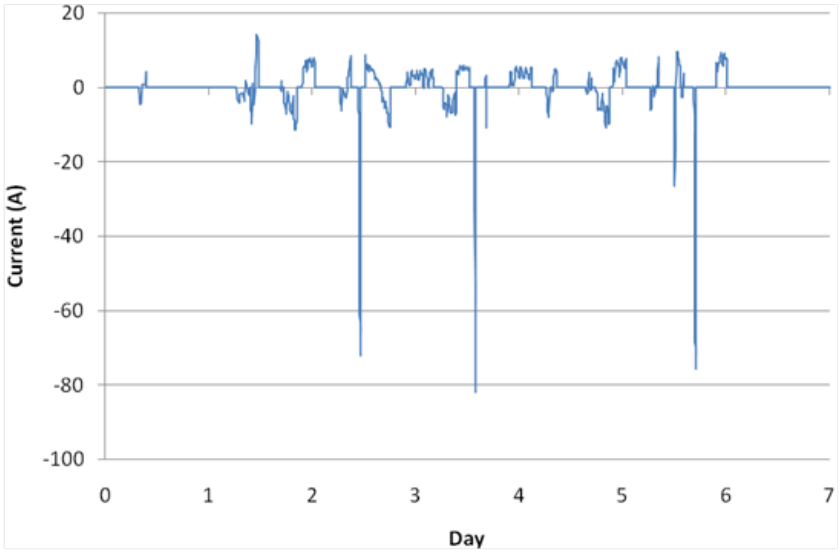

SOC: SOC is well controlled within the 0.2-0.95 range showed in Figure 32, and Lithium ion battery has a wider range of operational SOC up to 100% without capacity loss.

Figure 32: Battery Scouring the Week

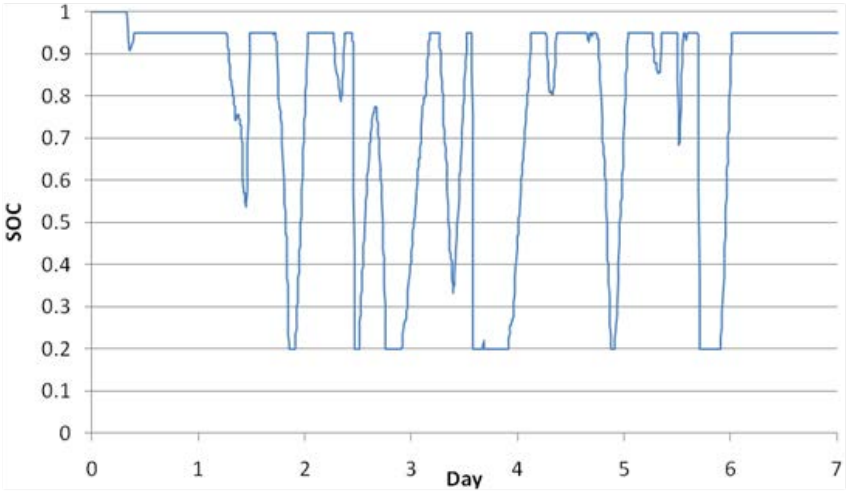

Battery power and System net power: Battery power is simulated and showed in Figure 33, and system net power is simulated and showed in Figure 34.

Figure 33: Battery Power During the Week

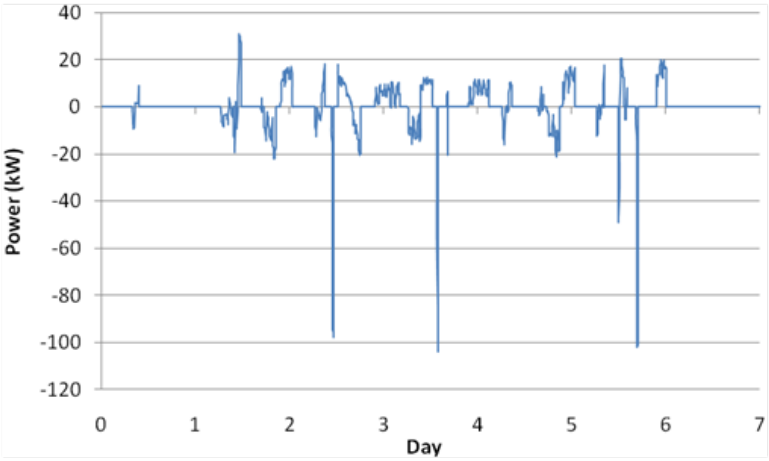

Figure 34: System Net Power During the Week

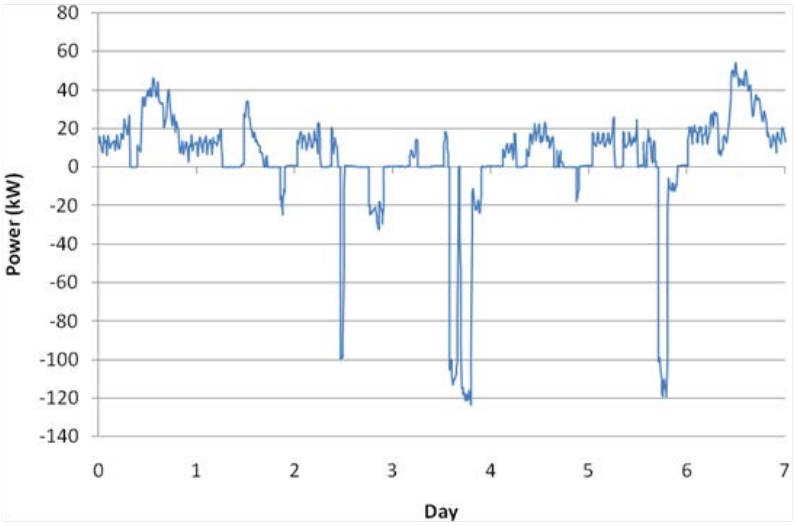

The results show that there is excess energy that cannot be stored in the system and peak loads that no power could supply to. To improve the current system in terms of excess power supply, either higher energy storage capacity should be provided to the system or less base load power supply from the grid. To meet the extreme peak power, ultra-capacitor bank can be implemented in the system and the battery & UC component can also be optimized.

CHAPTER 3:
Economic Dispatch of CCHP System Models Development

3.1 Electric and Natural Gas Rate Structure Models

3.1.1 Electric Rate Structure Model

Electric rate structures are typically broken down into fixed, energy (aka volumetric), and demand charges. The methods by which these charges are calculated vary amongst utilities and rate structures (e.g., time of use, declining block, and fixed or non-time of use rate). As a result, the calculation of charges can vary drastically between utilities and tariffs. It is therefore important to capture the general characteristics of an electric rate structure and how it functions as a whole, as opposed to specific individual charges associated with a particular rate structure.

For example, some common charges can be broken down into non-time of use (non-TOU) and time of use (TOU) charges. These charges often vary with season, with higher charges for seasons when total utility demand is highest. Non-TOU energy charges consist of a flat rate that applies to all of the energy consumed by a customer. Non-TOU demand charges are often determined by the largest load recorded for that billing period. As for TOU energy charges, they depend on what time the energy is consumed. TOU energy rates are generally highest during periods of high electrical demand ("on-peak"), lower for periods of moderate electrical demand ("mid-peak"), and lowest during periods of low electrical demand ("off-peak"). TOU demand charges are determined by the largest load recorded during a specific time period during the billing period. If a declining block rate is being used, the charge is reduced with increased electricity consumption. Many declining block rate structures are presented in a three tier structure separated by levels of electricity consumption, with electricity becoming progressively less expensive as the customer reaches each new tier. The electrical rate structures used in this work were based on the structures used by Southern California Edison (SCE).

SCE rate structures for commercial and industrial buildings are broken down by maximum yearly customer demand. Customers with loads greater than 20 kW are offered the choice between at least two different rate structure types: (1) TOU-A, which has larger energy charges than TOU-B; and (2) TOU-B, which has higher demand charges than TOU-A. Both rate structures contain TOU energy charges, and both TOU and non-TOU demand charges. SCE defines "summer" as June 1st through October 1st, and "winter" as all other times. During the summer, the on-peak hours are 12:00 p.m. to 6:00 p.m., the mid-peak hours from 8:00 a.m. to 12:00 p.m. and 6:00 p.m. to 11:00 p.m., and off-peak hours are all other hours. During the winter, on-peak hours do not exist, mid-peak hours are from 8:00 a.m. to 9:00 p.m., and off-peak hours are all other hours. Energy charges versus time of day for summer and winter season are shown for TOU8 in Figure 35 and Figure 36. Figure 36shows the percentage of a year for which each peak period is applicable. A non-TOU demand charge of $11.88 per kW is applicable for all months and is determined by the highest 15 minute average demand in a month. During the summer, TOU demand charges exist for both on-peak and mid-peak, and are $19.49 per kW and

$5.46 per kW respectively. These are determined by the highest 15 minute average demand during the peak period in a month. All SCE tariffs for buildings with maximum yearly load over 20 kW are shown in Table 6. The rate structures shown in Table 6 are applicable to customers who do not have Distributed Generation (DG).

Figure 35: Southern California Edison TOU8 Energy Charge versus Time of Day for Summer and Winter Seasons

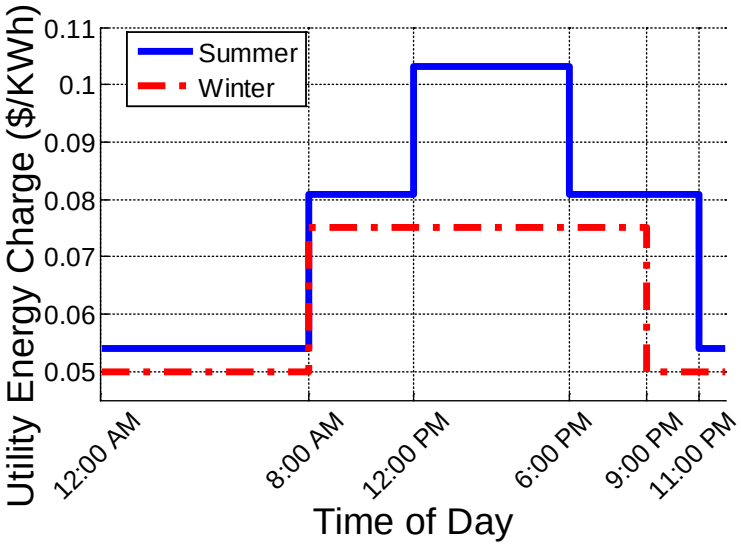

Source: Southern California Edison (SCE).

Figure 36: Percentage of the Year Comprising Each of the Southern California Edison Peak Periods

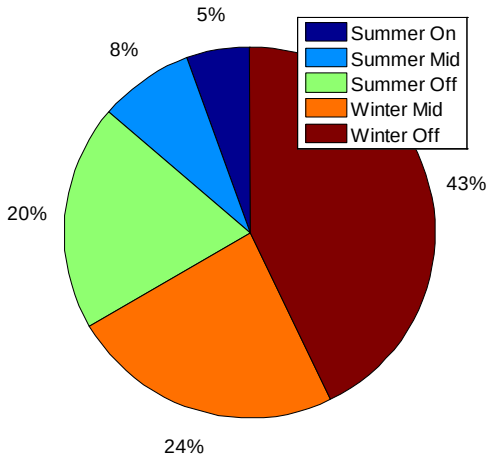

Source: Southern California Edison (SCE).

Table 6: Southern California Edison Energy and Demand Charges for Commercial and Industrial Buildings with Loads Larger than 20 KW

SCE Tariff			GS-2		GS-3		TOU8	
Applicable Building Size (kW)			20-200		200-500		>500	
Rate Structure Type			TOU-A	TOU-B	TOU-A	TOU-B	TOU-A	TOU-B
Energy Charges	Summer	On ($/kWh)	$0.37809	$0.13667	$0.28163	$0.11855	$0.36288	$0.10323
		Mid ($/kWh)	$0.14311	$0.08398	$0.12820	$0.08493	$0.13528	$0.08078
		Off ($/kWh)	$0.05511	$0.05511	$0.06507	$0.05950	$0.05407	$0.05407
	Winter	Mid ($/kWh)	$0.08066	$0.08066	$0.06992	$0.06394	$0.07505	$0.07505
		Off ($/kWh)	$0.05183	$0.05183	$0.05273	$0.04819	$0.04980	$0.04980
Demand Charges	Summer	Non-TOU ($/kW)	$12.18	$12.18	$13.30	$13.30	$11.88	$11.88
		On TOU ($/kW)	N/A	$14.94	N/A	$12.96	N/A	$19.49
		Mid TOU ($/kW)	N/A	$4.57	N/A	$3.08	N/A	$5.46
	Winter	Non-TOU ($/kW)	$12.18	$12.18	$13.30	$13.30	$11.88	$11.88

Source: Southern California Edison (SCE).

3.1.2 Natural Gas Rate Structure Model

Natural gas utilities usually sell their gas in a block structure. These block structures can have a single price for all gas used or be a three tiered declining block structure, with gas becoming progressively less expensive as the customer reaches each new tier. The standard charge is dollars per therm. Southern California Gas Company (SCG) is a major provider of natural gas to many of SCE's customers, providing a declining block structure for commercial and industrial users. Like many natural gas utilities, SCG's rates take into account the distribution and fuel costs. While distribution costs have been observed to be relatively stable for SCG, fuel costs regularly change depending on the price of natural gas. As a result, while natural gas rate structures are relatively simple, changes in fuel cost cause regular changes in customer prices. Prior work has shown that fuel price has a large impact on distributed generation economics. However, due to increased reserves and production of natural gas, prices have been "depressed… to the lowest levels in a decade"[17], leading to price projections that remain low in the near future[18]. While energy price projections have been shown to be inaccurate[19], a

[17]Gilbert, D., Fowler, T., **Natural Gas Glut Pushes Exports**, Wall Street Journal. 2012: U.S. Edition.

[18]United States. Office of Energy Markets and End Use. and United States. Energy Information Administration. Office of Integrated Analysis and Forecasting., **Annual Energy Outlook. 2012**, The Office: Supt. of Docs., U.S. G.P.O., [distributor]: Washington, D.C. p. v.

distributed generation investment that pays back in a reasonable time period should reduce the risk of exposure to natural gas price volatility. As a result, the natural gas rate model will follow SCG prices effective June 10th, 2012. This rate structure is as follows: $0.81115 for the first 250 therms, $0.56622 for the next 3,917 therms, and $0.402 for all other therms.

3.2 Finance Models

A finance model was developed in order to determine the appropriate cost of capital associated with investment in DG, track the cumulative costs of energy, and determine the simple payback of the investment.

The cost of capital associated with investment in DG would come in the form of a loan used to assist the purchase of the DG. It was assumed that the loan would cover 80% of the purchase cost of the equipment and the other 20% would be funded directly by the investor. The cost of this loan to the investor was summed up in a monthly debt payment, calculated through the following equation:

$$\textbf{Monthly Debt Payment} = \frac{\textbf{Principal} * \textbf{i}}{\textbf{1} - (\textbf{1}+\textbf{i})^{-\textbf{n}}}$$

where i is the interest rate, principal is the total loan amount, and n is the debt term. For this study, the interest rate was set to eight percent and the debt term was set to 10 years.

The cumulative cost of energy was determined first by using the electric parent rate structure and natural gas rate structure to determine the baseline case (no DG) for the cost of energy. Then, after the dispatch strategy had been applied to the building load using the generator specifications assigned to the model, the cost of energy was calculated using the electric standby rate structure, natural gas rate structure, and determining the O&M from the generator dispatch. These costs were summed and compared to the baseline case, allowing for the monthly savings to be calculated. These savings were used to represent future energy savings also. The cost of capital was then applied through the life of the loan, allowing for savings including capital costs to be determined.

Many investment criteria exist for judging the quality of DG investment[20]. The criteria picked for this study was simple payback. While other criteria include the time value of money, simple payback is a good indicator of investment potential; other criteria do not give positive investment reviews unless simple payback occurs in a timely manner.

Since cost of capital is included through the first ten years, payback lengths that do not occur within this time frame can have exaggerated paybacks due to this additional cost that stops at the end of year ten. As a result, payback is determined to occur when the cumulative savings,

---

[19]Smil, V., **Perils of Long-Range Energy Forecasting: Reflections on Looking Far Ahead.** Technological Forecasting and Social Change, 2000. 65(3): p. 251-264.

[20]Biezma, M.V. and J.R.S. Cristóbal, **Investment Criteria For the Selection of Cogeneration Plants - A State of the Art Review**. Applied Thermal Engineering, 2006. 26: p. 583-588.

starting with the initial 20% of the purchase price invested, is greater than zero and does not subsequently turn negative.

CHAPTER 4:
Central Plant Installation and Performance Verification

The central plant at UCI is staffed by licensed Steam Engineers and is operational 24/7, serving the following purposes:

- Produce and distribute chilled water (for cooling, dehumidification, and process cooling), high temperature hot water (for building heating water, domestic and industrial hot water, low-pressure steam generation for research equipment) and compressed air (for instrumentation and automation functions and for research laboratories) to campus buildings
- Produce and distribute electricity via the cogeneration plant (CHP - Combined Heat and Power)

The central plant is the heart of the utility infrastructure of the campus. Its schematic diagram is in Figure 37.

Figure 37: UCI Central Plant Diagram

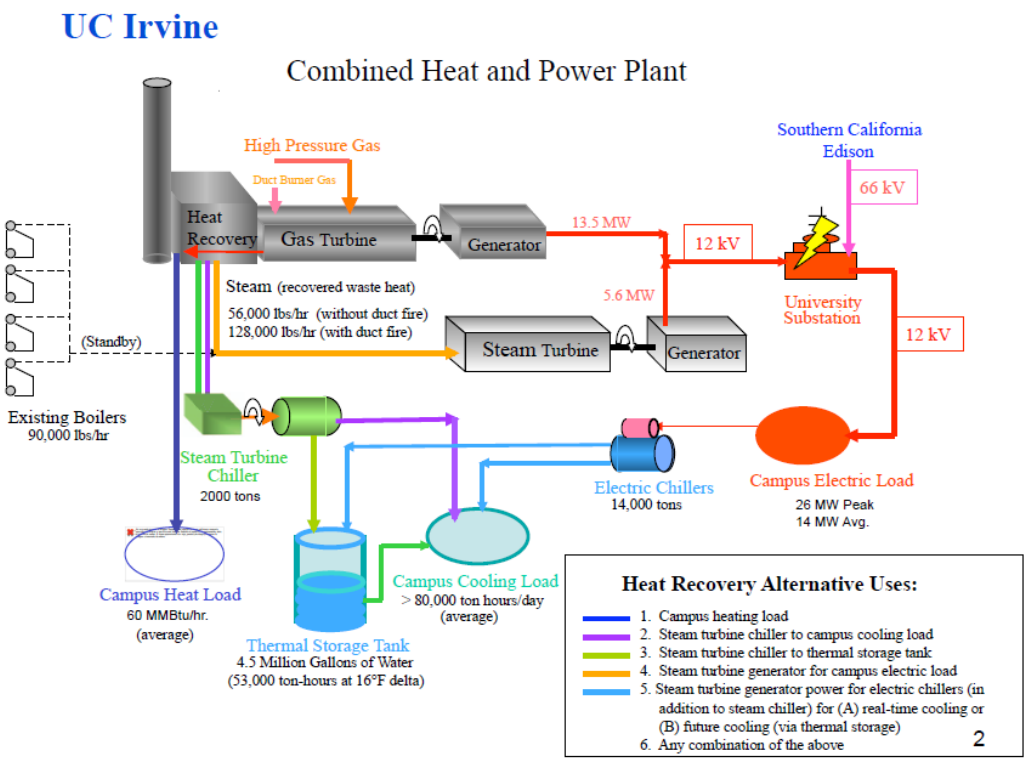

4.1 Operations at the Central Plant

4.1.1 Summary of Operations

1. Set-points for the chillers are only on-off; there are not many other parameters to set, except that the flow rate through each chiller can be adjusted (by changing set-point for the chiller pumps).

2. Chillers are turned on and off during the evening, but between 6am and 11pm there is usually no turning on of any chiller. This is because turning on chillers will lead to large spikes (MW level) in the electricity consumption profile, and the associated demand charge is what the operator try to avoid. However, it is ok to turn off chillers during daytime.

3. According to Dennis, if one chiller is turned on, it takes 30mins for it to reach full capacity. So if 3 chillers must be online at 6am, they should be turned on before 5:30am otherwise it will be late. However John confirmed that the electrical chillers are very fast in terms of response. After issuing the "start" command to an electrical chiller, it only takes a few minutes before it produces cold water. What is time consuming is the starting of the absorption chiller.

4. If towards the end of a day the TES does not have enough water to serve campus need, operator will have to turn on a small chiller which creates smaller spikes to the electricity consumption profile.

5. The TES is operated in a heuristic manner. Based on the level of thermo-cline and future expected TES discharging flow rate, the operators decide how to charge TES. They try to avoid consuming all chilled waters in TES (it is recommended to always leave more than 20 feet thermo-cline level). However different operators have their own style, some may be more aggressive.

6. The flow rate to/from campus and TES cannot be set directly. Instead, the differential pressure (DP) of campus loop is a set-point. The recommended DP set-points are given according to outdoor temperature:

Table 7: DP Set-points

Outside Temperature (F)	DP set-point (psi)
<65	10
65~75	11
76~80	12
81~85	13
85~88	14
>88	15

The secondary pumps are automated to maintain this set-point. This way the campus will suck water from the system and if more chilled water is produced it is sent to TES. If less water is produced the TES will discharge water to fill the gap.

7. When the return water temperature to chillers is low, it will put more flow on chillers (can be 20% higher than max design value). Chillers do not do a lot of cooling job but mainly to pass water flow through. Also to deal with high cooling demand in the afternoon, the operators do not want to turn off too many chillers in the morning (usually 2~3 will remain online) because that way when it is necessary to bring them back on-line big spikes will be created in the electricity consumption profile.
8. There are many valves in primary and secondary loop, whose percentage of opening can be controlled by operators.
9. Several chillers they have are dual chillers, meaning that they are actually a combined unit of two chillers. For example chiller 5 has two chillers 5-A and 5-B, each one has its own pump and peripheral components. They can be turned on and off independent of each other. But this is rarely done in practice. The design parameter for some of the chillers are as follows

Table 8: Chiller Specifications

	Evap gpm	Cond gpm	Evap DT	Cond DT
Chiller #4	2850	4650	17	12
Chiller #5	3750	7500	15	10
Chiller #6	3750	7500	16	10
Chiller #7	4500	9000	16	9.5
Chiller #8	4500	9000	16	9.5

10. Absorption chiller, steam turbine and campus hot water system all consume steam that is recovered from co-gen. The temperature of hot water supply to campus is set to constant set-point. The steam flow is also pressure controlled.

4.1.2 Existing CCHP Plant

In almost all power plants, a historian database is setup to record and monitor plant processes. The most common databases found in the industrial or utility plants are structured query language (SQL) databases – more commonly used due to its competitive pricing despite lower compression rate as compared to their less successful counterparts, procession historians. For this project, the performance and operational routines of an existing CCHP plant, including its required energy profiles were queried from an in-plant SQL database. The query was made by utilizing the WonderWare, data-acquisition software interface, through serial connection from

an external computer. For the most part, historical data collected from the existing CCHP facility were at 15-minute interval continuously for at least a calendar year.

Figure 38: Schematic of Plant Layout and Connectivity to Campus for UCI Central Plant

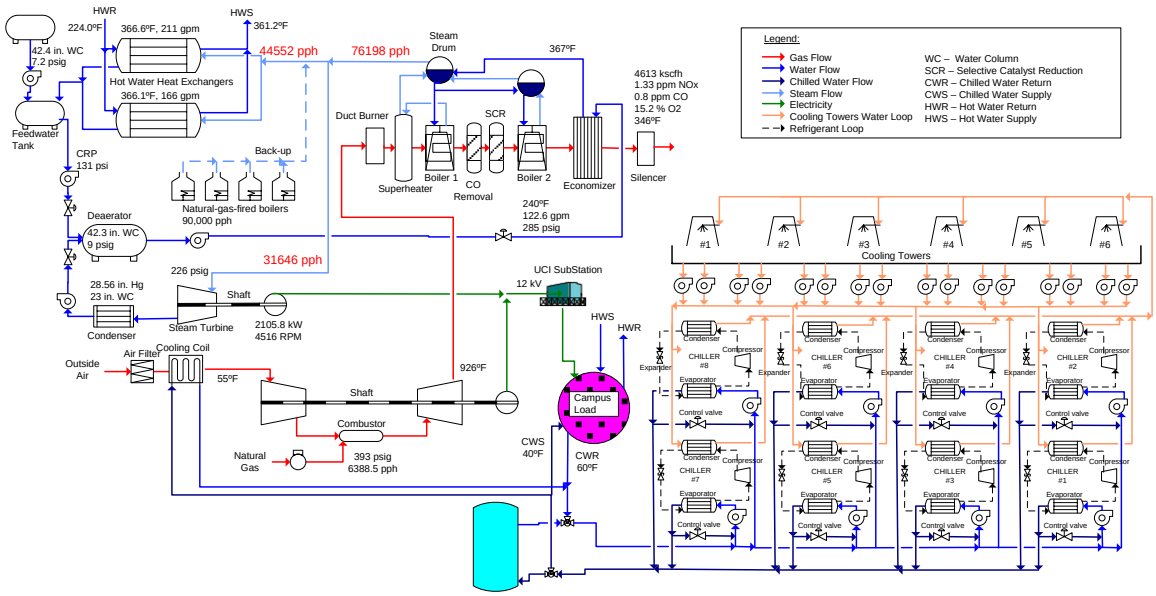

The CCHP plant at the University of California, Irvine (illustrated in Figure 38) is selected as a case study to:

- Verify model dynamic performance
- Assess novel operating strategies and controls
- Predict various energy management scenarios

The UCI Central Plant is a cogeneration plant serving the campus with power, hot water, and cooling capacity. Originally intended as a steam plant, the facility was designed with natural gas-fired boilers and steam chillers to provide district heating and cooling for the campus. It was expanded in 2007 to meet campus growing needs, reduce its energy bills and at the same time reduce campus carbon footprints. The expansion made good economic and operational sense to the central plant, as it added a gas turbine and HRSG unit to the existing infrastructure and existing transmission.

The remodeled plant is a scale-down version of a large scale CCHP plant that involves a gas turbine as a prime mover, a HRSG compartment for steam generation, and a thermal energy storage (TES) tank for load shifting. Most of the older steam chillers were phased out and replaced by electric chillers. Cooling was supplied to campus in parallel with cold storage with TES tank. This configuration effectively plateaus campus daily electrical demands and allows the gas turbine to operate at high part-load for most of the year. With very few scheduled shutdowns and startups sequence, the plant experiences transient conditions during chillers operational sequence. The starting up and shutting down sequence of electric chillers each rated between 1 to 2 MW.

4.2 Equipment Installed at the Central Plant

1. An industrial computer with reasonable ROM and RAM, sufficient data acquisition capability, communication ports, and computing capabilities has been installed.
2. A Siemens "Smart Energy Box" with computing capabilities that include the novel controls developed in the current project has been installed.
3. An industrial "touch-screen" display of the results from the current control strategies and novel optimization techniques for the "man-in-the-middle" control that is used in the current effort has been installed.
4. All of the communication cables, connecting hardware and power cords associated with the above equipment has been installed.

4.3 CCHP Energy Demands

The dynamics experienced by the plant are generally of two categories, (1) campus energy demands mostly attributed by normal working hours and ambient conditions throughout the day, and (2) starting-up and shutting down of electric chillers. Campus energy demands though seasonal, typical follow the pattern of high heating loads in early morning, peaking power and cooling demands from noon to early afternoon.

The University of California, Irvine locating in the South Coast Air Basin region (under the AQMD distinction) enjoys a Mediterranean climate. The area is subject to rainy winter and dry summer and rarely affected by weather extremes such as hurricanes, tornadoes, storms, etc. However, it is affected by coastal weather phenomenon called June Gloom, which is weather pattern that caused by the marine layer sweeping in land. This results in overcast skies and foggy conditions starting early morning and can last until the afternoon. The June Gloom season usually starts in late May and ends in early July. Thus, ambient temperature of the campus is highly dictated by this annual occurrence.

Figure 39: Ambient Temperature Profile in Degree Fahrenheit for UCI Campus for Calendar Year, 2010

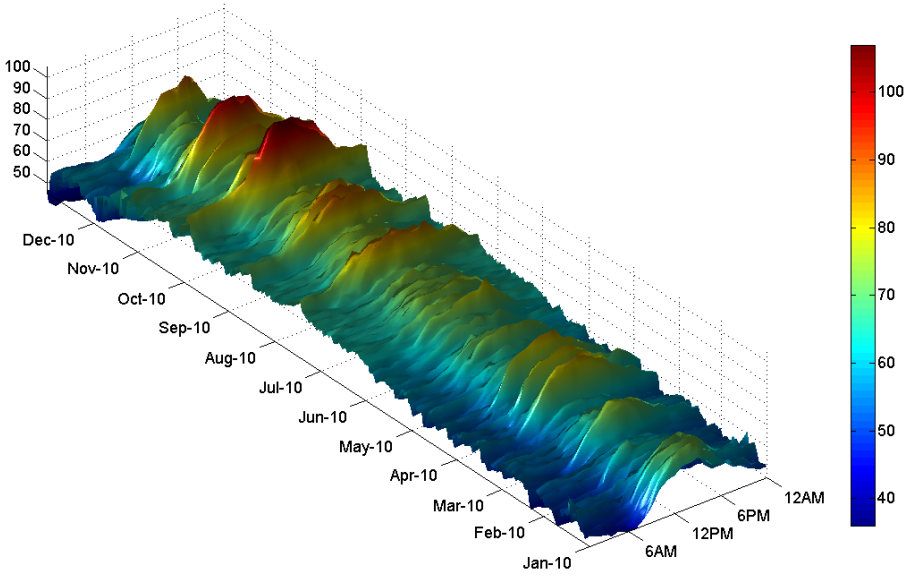

Figure 39 displays the historical weather data for the calendar year 2010. The data were collected from a nearby weather station at 1-hour resolution. As can be seen from the plot, the early summer period from May to early July experienced mild average daily temperatures. At the onset of first heat wave in mid-July, average temperature increased with a few occasions of unusual heat waves occurring in early October and early November. This temperature variation is important to the operation of the Central Plant as it sheds light on the energy demand patterns of the campus. Different mode of operation can be selected based on different climate regimes such as listed below,

1. Low daily temperatures in early to mid-summer coupled with lower campus occupancy due to summer schedule signifies low energy demands
2. High daily temperatures from September to November coupled with high campus occupancy signifies high energy demands
3. December observe the lowest daily energy demands due to winter holidays and low temperatures
4. Average energy demand profiles are expected for the months between January and May

Figure 40: Campus Total Electrical Profile in kw For 2010

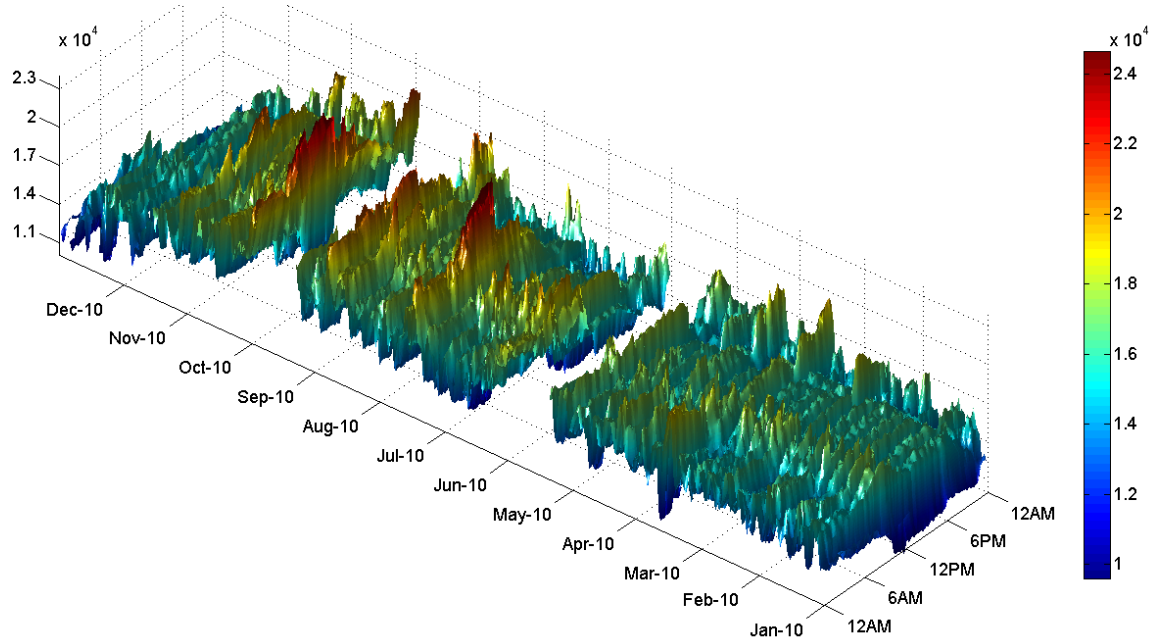

Figure 40 provides the net electrical demand history for the UCI campus for calendar year 2010. The data were collected from a historian database at UCI Central Plant. A structured query language (SQL) interface was used to query the data.

Figure 41 displays the daily energy demands of UCI campus which exemplifies the typical energy supply and demand patterns. As can be seen from the figure, rising heating demands start in the early morning that peaked at between 8 and 9 AM. The peaking heating demands are adequately met with steam generated by the HRSG with the gas turbine running full-load. The heating load is calculated from historical data of the supply and return flow rates of the hot water produced by the Central Plant to service the campus. The heating load formula is

$$\dot{Q}_{HW} = \dot{m}_{HW} \rho c_P \left(T_{HWS} - T_{HWR} \right)$$

where

$\dot{Q}_{HW}$ = Energy rates supplied by heating loop in kW

$\dot{m}_{HW}$ = volumetric flow rates of hot water in m^3/s

ρ = density of hot water in kg/m^3

c_P = density of hot water in $kJ/kg \cdot °C$

T_{HWS} = temperature of hot water supply by Central Plant in $°C$

T_{HWR} = temperature of hot water return by Central Plant in $°C$

Although the temperature range of hot water supply and return flows is between 200 to 370°F (equivalent to 93 to 188°C), the flows are compressed at high pressure (300 psig for supply flow and 260 psig for return flow at the Central Plant). Due to this aspect, the compressed water is very likely to remain liquid phase. Thus, properties of the hot water are approximated as those at standard conditions.

Figure 41: Energy Demand Profiles of UCI Campus over the Early Days of January 2010

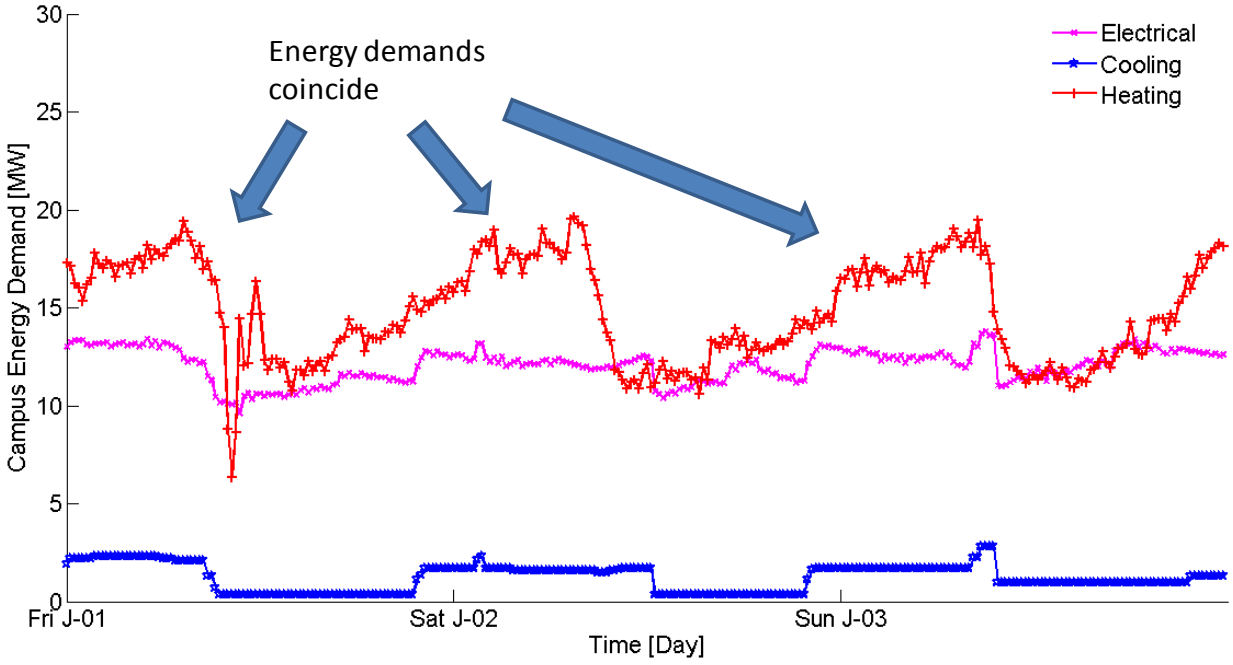

The cooling demand in Figure 41is determined from historical records of chillers' cooling load in refrigeration ton-hours. Recorded performance of the chillers are provided in cooling tons, which can be converted to power consumption based on rated chillers' performance. Table 9 tabulates the performance information for all 8 chillers available at UCI Central Plant. The kW/Ton column is a result of dividing the rated compressor maximum power by the rated capacity of that chiller. The coefficient of performance (COP) value is evaluated by dividing the kW/Ton term into the conversion factor of 3.516.

Table 9: Nameplate Capacity and Refrigerant Type for All Chillers Employed at UCI Central Plant

Chiller #	BRAND	MODEL	Ref.	Rated Capacity (Ton)	Compressor Max Power (kW)	kW/Ton	COP
1	Trane	CVHE11200P	R123	1120	653	0.648	5.4
2	Trane	CVHF1280	R123	1280	745	0.739	4.8
3	Trane	CVHF1280	R123	1280	745	0.739	4.8
4	YORK	YKWHVDJ4	R134a	2000			
5	Trane	CDHF2500	R123	2500	1300	0.516	6.8
6	Trane	CDHF2500	R123	2500	1300	0.516	6.8
7	YORK	YDYHYAJ3	R134a	3000	2030	0.672	5.2
8	YORK	YDYHYAJ3	R134a	3000	2030	0.672	5.2

Note: All are electric-driven with exception of steam-driven chiller #4, which was not used for 2009-2010 due to maintenance issues.

The critical dynamics essential to plant operation and thus gas turbine operation are those associated with operating the electric chillers. These chillers perform well close to the operational point of the highest COP (coefficient of performance). This dictates that they would exert 90% or more of their rated power consumption. Therefore, the on-and-off operation of the chillers directly affects the dynamics of the power load at the plant. Under the current interconnection agreement for the gas turbine, the engine (Solar proprietary control interface) handles large load sheds through automated controls while manual control is managed by plant operators with regards to plant load increases due to import imposed by the regional utility, Southern California Edison (SCE). The interconnection agreement is a stand-by connection criteria that requires UCI Central Plant to import 1 MW of electricity at all times from SCE. This criteria effectively inhibit the campus from exporting electricity.

Individual chiller power consumption is calculated by multiplying the recorded cooling production of each chiller (such as shown in Figure 42) to the rated kW/Ton. Each recorded data point in the figure represents a 15-min averaged data queried from the SQL database serving as the Historian of plant performance. Several key takeaways can be drawn from Figure 42. The first is Chiller #5 was operated at night primarily to charge the bulk of the TES tank. Along with its twin Chiller #6, Chiller #5 has the highest COP value and should be the most electrically efficient with very capable cooling capacity to produce campus cooling demands in the winter. Chillers #1-3 with smaller capacities and slightly lower COP values are used as backup generators to account for the cooling demand unaccounted for when Chiller #5 or #6 is on (in the winter). Another important observant is there seems to be signs of indecision on the part of the Central Plant operators. For instance, in the early morning of Saturday Jan 2nd, Chiller #2 was started-up and operated for only 30 min before its eventual shutdown. This is could have

been due to plant operators deciding at first to operate the plant the same as the previous day, before realizing campus demand for the Saturday might not necessitate the extra generation from Chiller #2. Another instance of operator's indecision occurred near mid-day of Sunday Jan 3. The operator started both Chiller #2 and #3, both 1000-ton machines, in replacing the production of the 2500-ton Chiller #5. An hour after, Chiller #5 was brought off-line along with Chiller #2, leaving #3 as the only one generating throughout the day. Such indecision could be avoided with the assistance of model predictive control (MPC) modules that can readily advise the operators the best course of actions at the moment.

Figure 42: Cooling Load Profiles for Individual Chillers at UCI Central Plant for a 3-day Period from Jan 1 to Jan 3, 2010

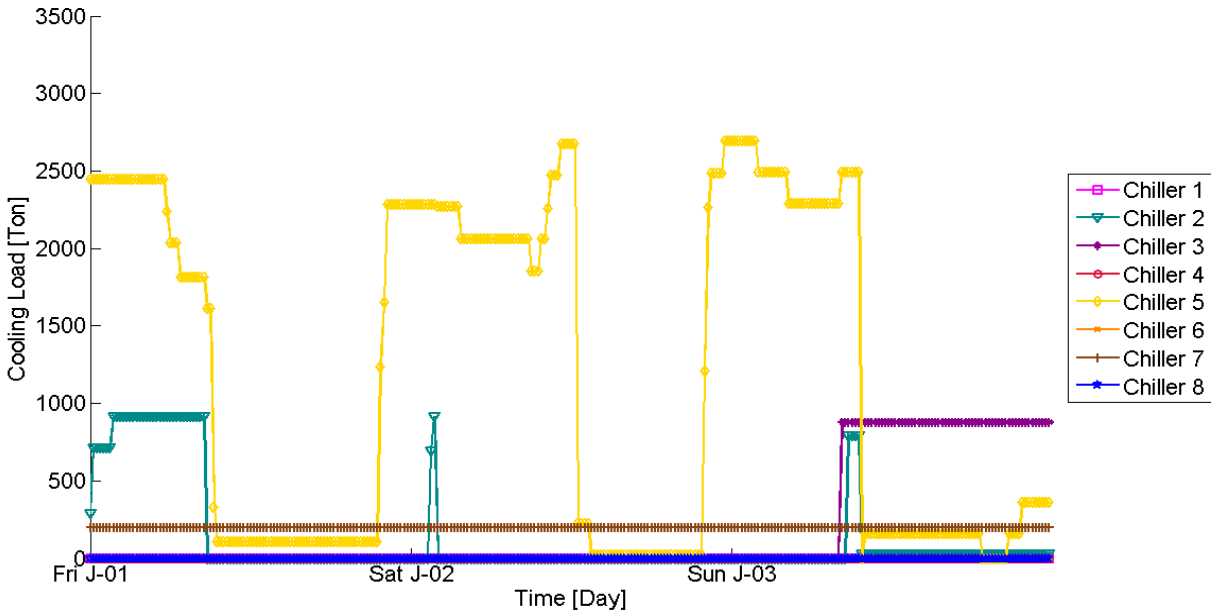

CHAPTER 5:
Installation and Operation of Novel Control Systems

5.1 Graphical User Interface for Analysis of Data for Model Predictive Control

A simple graphical user interface (GUI) was created to facilitate modeling and analysis of available data. The following sequence of figures illustrates the use of the GUI to analyze summer data collected for the APEP building, including weather, occupancy, set points and corresponding energy consumption values.

Figure 43 is the initial screen that appears upon execution of the file "setup.m" in the Matlab environment. It contains general instructions as to how to interact with the GUI to perform the analysis. Selcting "NEXT" in this menu opens the Excel file selection menu, Figure 44.

Figure 43: Model GUI on Start Up

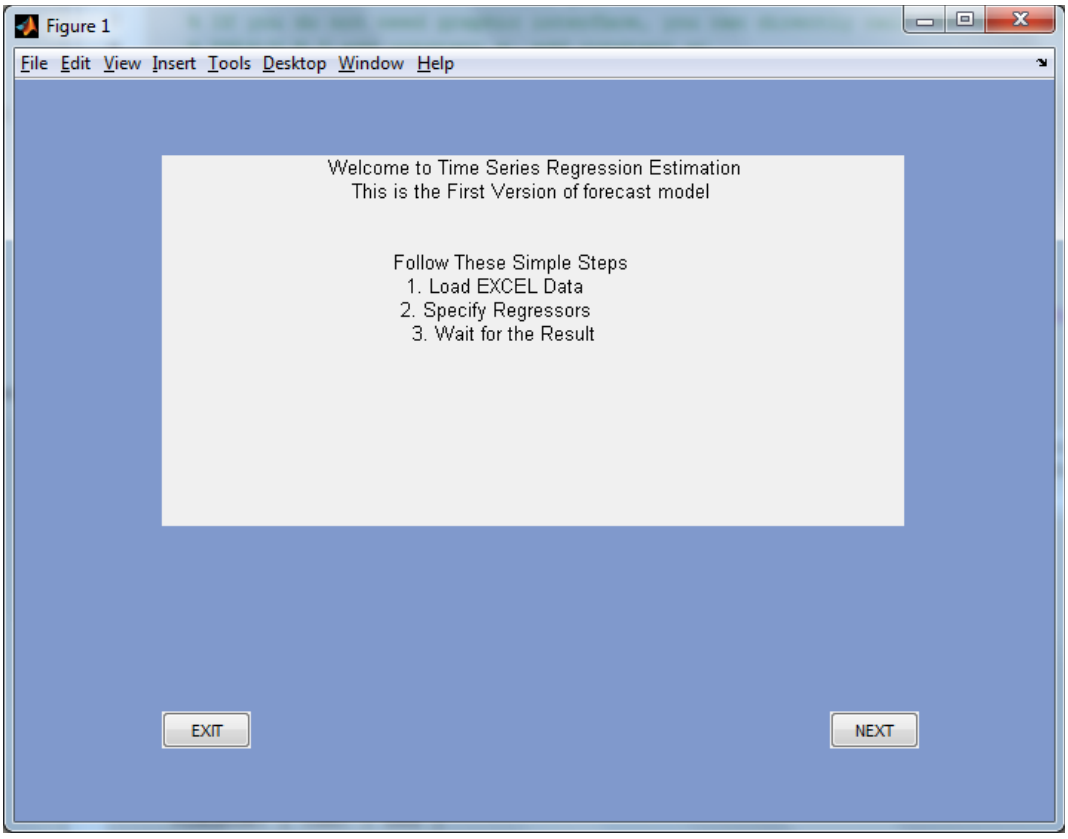

The Excel file selction menu allows the user to import stored building data into the working environment for subsequent analysis. In this example, the imported Excel filename is "`SummerForGUI.xlsx`." Users can browse files using the tab to the right. After the desired menu is selected, the user then selects "NEXT" to proceed to the next menu.

Figure 44: Excel File Selection Menu

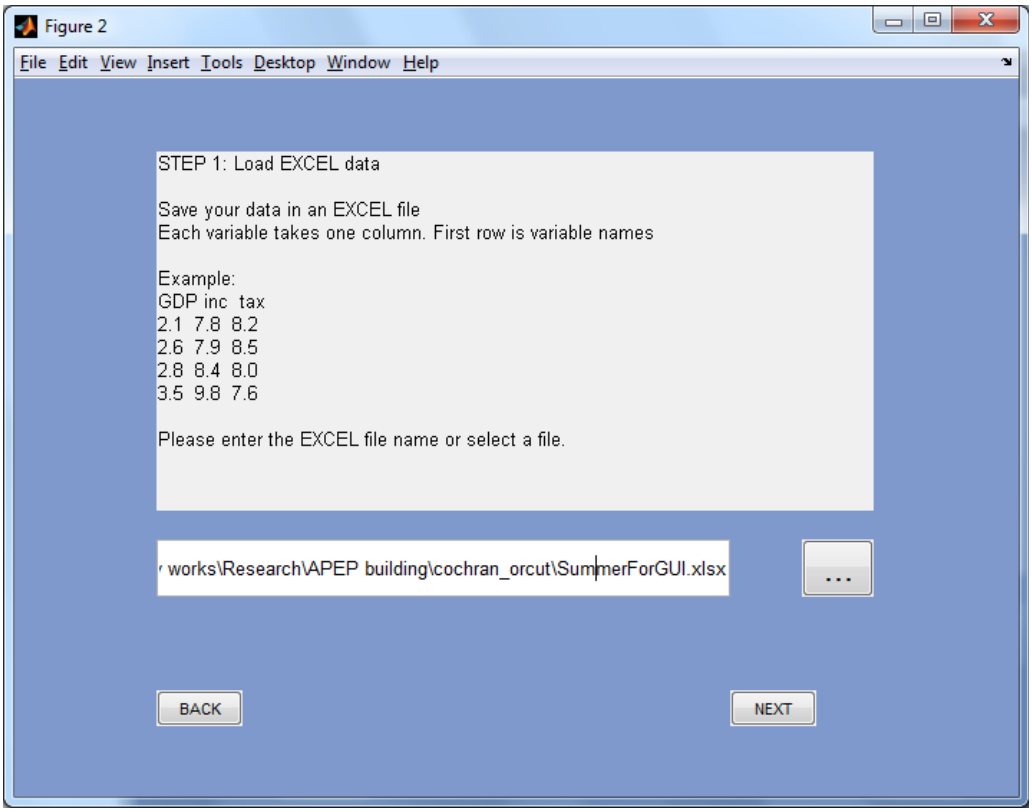

The next GUI menu, Figure 45, requires that user set the various parameters needed to perform an autoregression analysis on the dataset. This will include specifying the dependent (response) variable in the dataset as well as the independent (regressor) variables used to predict the response. Additionally, the user will be required to specify the order of the autoregression, i.e. the number of data lags included in the model, and whether or not to include intercepts.

Figure 45: Specifying the Model Parameters

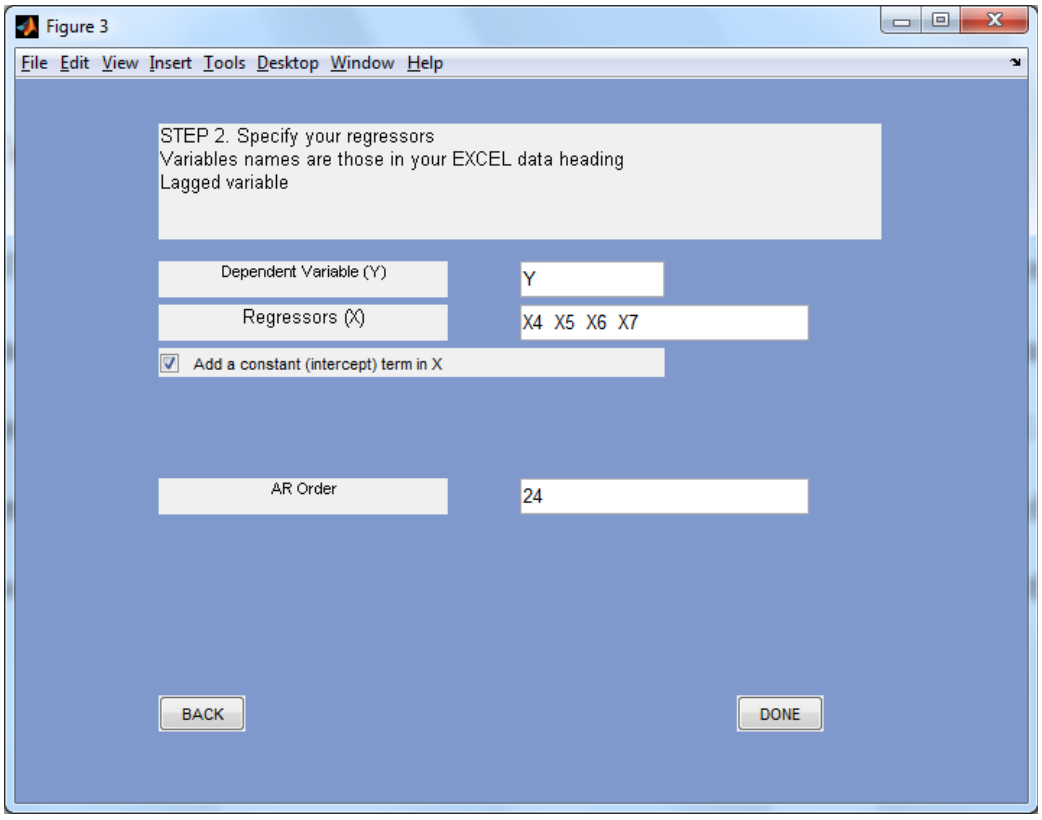

After specifying the model parameters, clicking "DONE" will execute the Cochran-Orcutt algorithm for finding the best estimation for all regression and time series parameters. It also returns the prediction and forecasted values. Here is a typical set of the results:

```
Regression Parameters-----------------------------------

  Beta Estimates      SE
 -3.1133e+005        15408
        27309       759.74
      -19.483       14.441

Time Series Parameters----------------------------------

  Phi estimates     SE
      0.65598     0.048262
```

```
 0.016413     0.059454
 0.013587     0.059437
-0.074702     0.059342
-0.078413     0.054273
 0.030197     0.050525
 0.032196     0.050451
 -0.10079     0.050472
  0.10925     0.050651
0.0096871     0.050424
 0.021434      0.04962
 -0.12497     0.049767
 0.034125     0.049726
-0.045079     0.049512
  0.12166     0.049373
 -0.10059     0.049726
 0.029589     0.049912
 0.054432     0.047986
-0.036056     0.047756
 0.067081     0.047423
-0.036432     0.047383
-0.0092797    0.047297
 0.082882     0.047172
  0.21158     0.039972


Model Quality ----------------------------------------------

      R Squared     R_squared(Adj)
       92.621       92.436
```

In these results, Beta values are estimates of the regression model and SE values are the corresponding standard errors. For the time-series Phi values and SE are estimates of auto-

regressive model and their corresponding standard errors. The `R Squared` and `R_squared(Adj)` are two measures for adequacy of the proposed model. Here, the regression time-series model together can explain about 92% of all variations.

The following figures depict the real and predicted value of energy consumption using training and validation dataset, respectively. In order to change the sample size for training dataset, one can change the variable `Learning_data_size`in`RunitByGUI1.m`

Figure 46: Real and Forecast Energy Consumption Data Using Training Dataset for APEP Building, Summer 2010

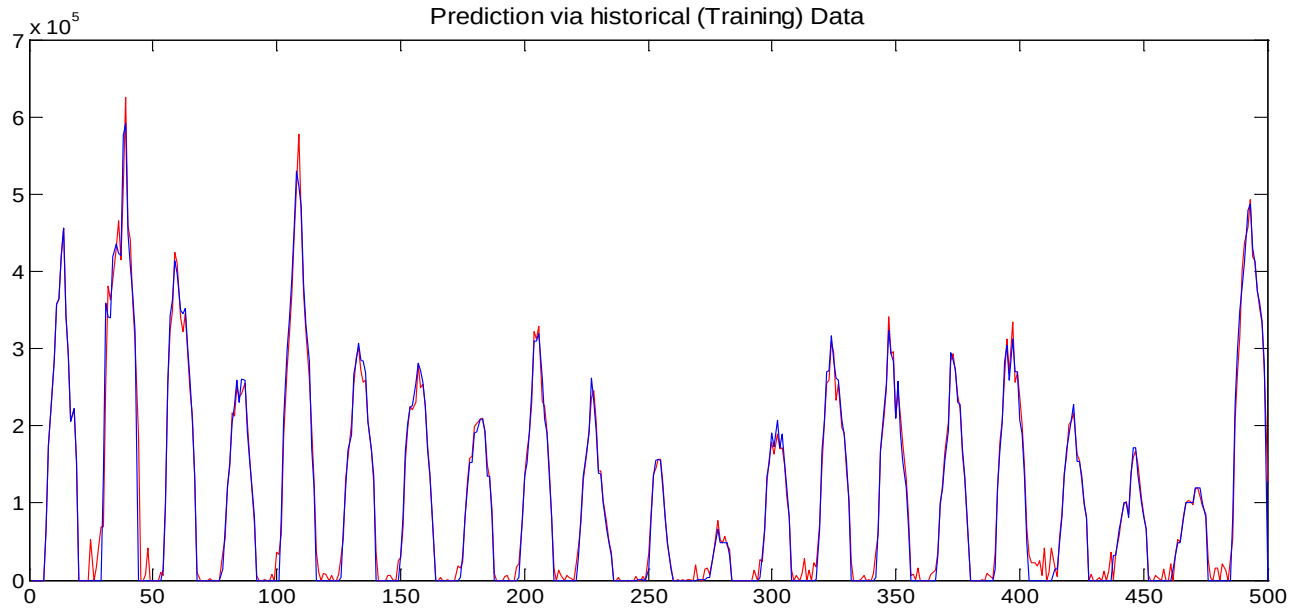

Figure 47: Real and Forecast Energy Consumption Data Using Validation Dataset for APEP Building, Summer 2010

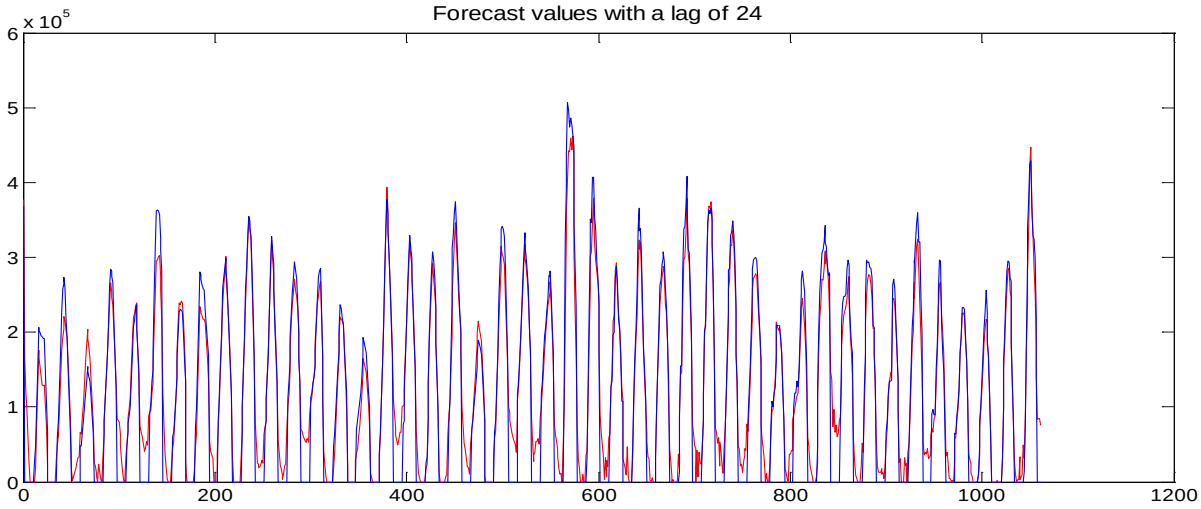

It is also possible to run the model directly through the codes and without using graphical interface. In doing so, it is easy to change any parameters of the model and the user is able to set their own preferences. To do this, one should run theMatlab file named "Runit". It is required to update the address of the dataset in the following part of the code:

```
Data = xlsread('\Summer.xlsx');
```

This should be changed by new location of the dataset.

Note that "Runit" calls another function which is Cochrane_Orcutt_test1 to perform the Cochrane-Orcutt algorithm for AR(*p*) case. If the model is more complex, one can change the following part of the code:

```
 [Beta,SE,AR_para,SE_AR,resid_final]=
Cochrane_Orcutt_test1(Y(1:Learning_data_size),X(1:Learning_data_size,:
),add_constant,AR_lag,max_iter);
```

with

```
[Beta,SE,AR_para,SE_AR,resid_final]=
Cochrane_Orcutt_test2(Y(1:Learning_data_size),X(1:Learning_data_size,:
),add_constant,AR_lag,max_iter,fixAR);
```

leading to invoke Cochrane_Orcutt_test2 function which supports all seasonal ARIMA model. `Cochrane_Orcutt_test2`also needs to redefine some settings based on the ARIMA or GARCH models.

5.2 Preferred Daily Operation Routines for Critical Peak Pricing Events

One of the most critical parts of UCI Central Plant operation is the dispatch of the chillers (1-8). The current set of research highlights focuses upon the various ways in which the chillers could be dispatched to take advantage of "Critical Peak Pricing" events. The following figures summarize the dispatch of all eight chillers (Chiller #1 – Chiller #8) for various cases, each of which take advantage of "critical peak pricing" rate structures.

Figure 48: Business-as-Usual Operation of Chillers for the Selected CPP Day of July 14, 2010

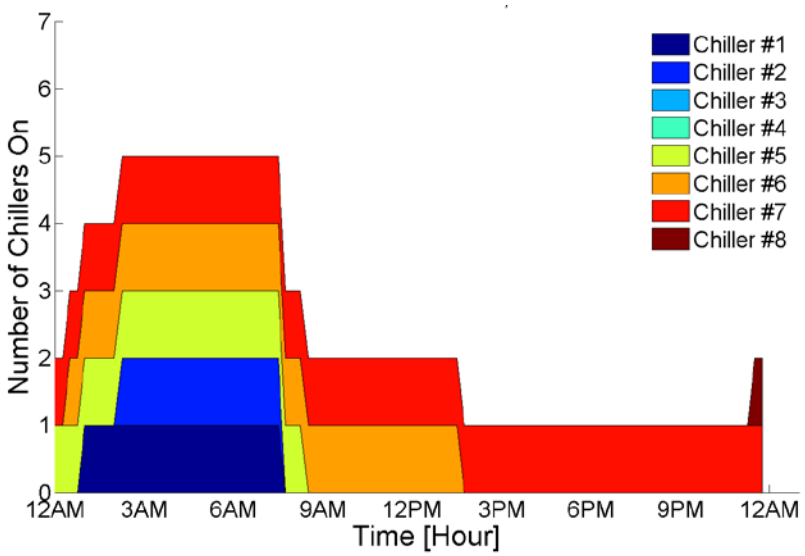

Note: Chiller online status is '1' while off-line is '0'

Figure 49: Business-as-Usual Operation of Chillers for the Selected CPP Day of July 16, 2010

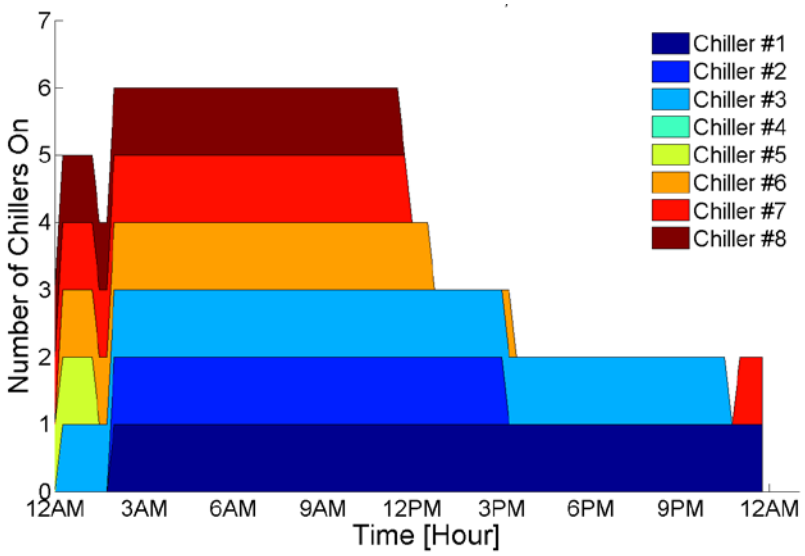

Note: Chiller online status is '1' while off-line is '0'

Figure 50: Simulated Novel Dispatch Chillers to Displace Electrical Load during CPP Window for July 16, 2010

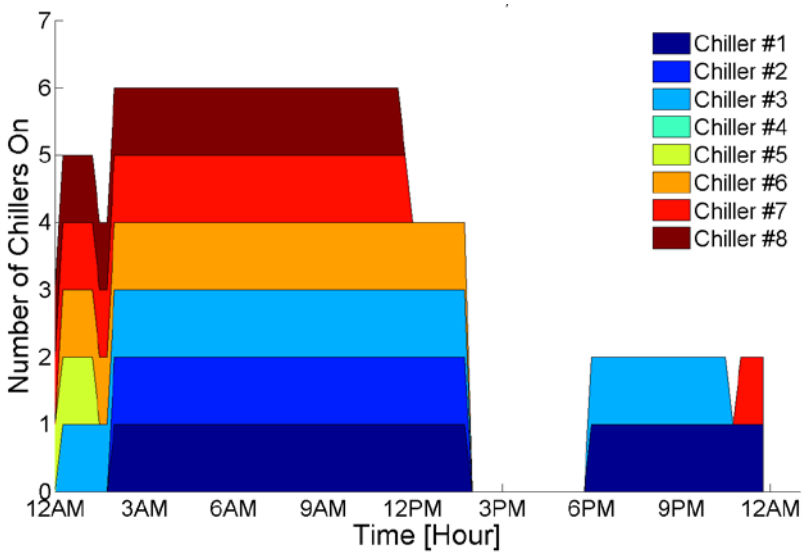

Note: Chiller online status is '1' while off-line is '0'

Figure 51: Business-as-Usual Operation of Chillers for the Selected CPP Day of August 18, 2010

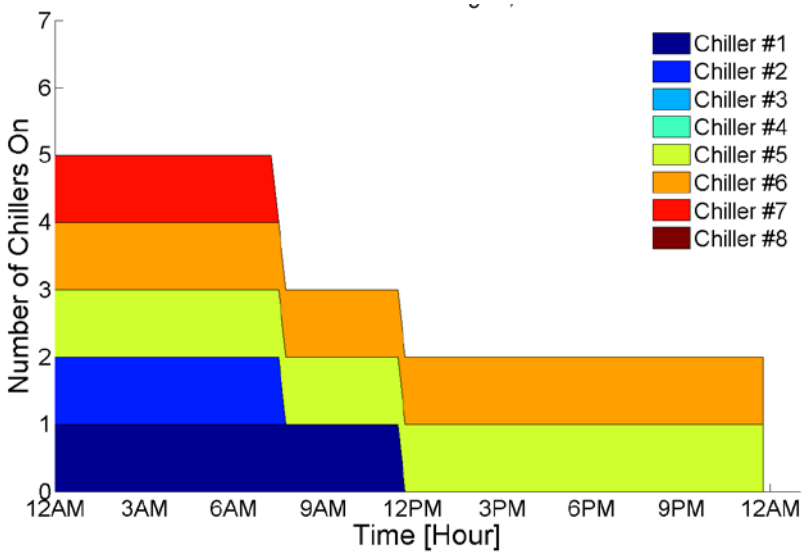

Note: Chiller online status is '1' while off-line is '0'

Figure 52: Simulated Novel Dispatch Chillers to Displace Electrical Load during CPP Window for August 18, 2010

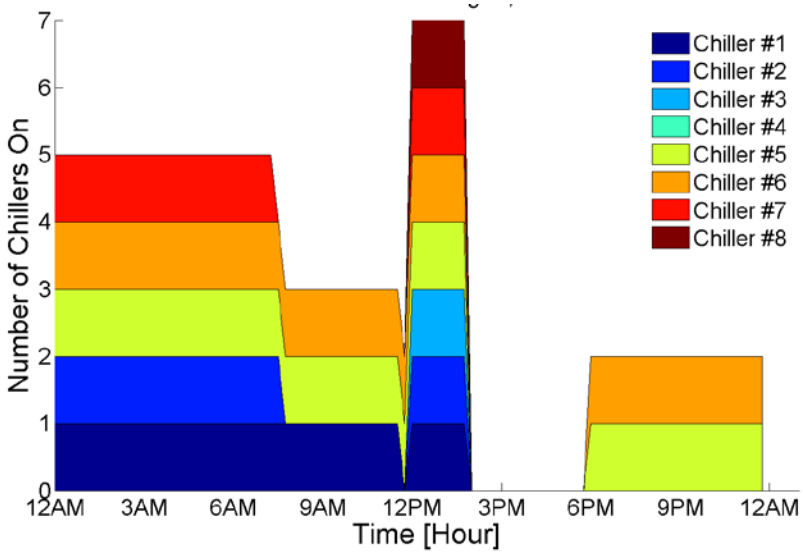

Note: Chiller online status is '1' while off-line is '0'

Figure 53: Business-as-Usual Operation of Chillers for the Selected CPP Day of August 23, 2010

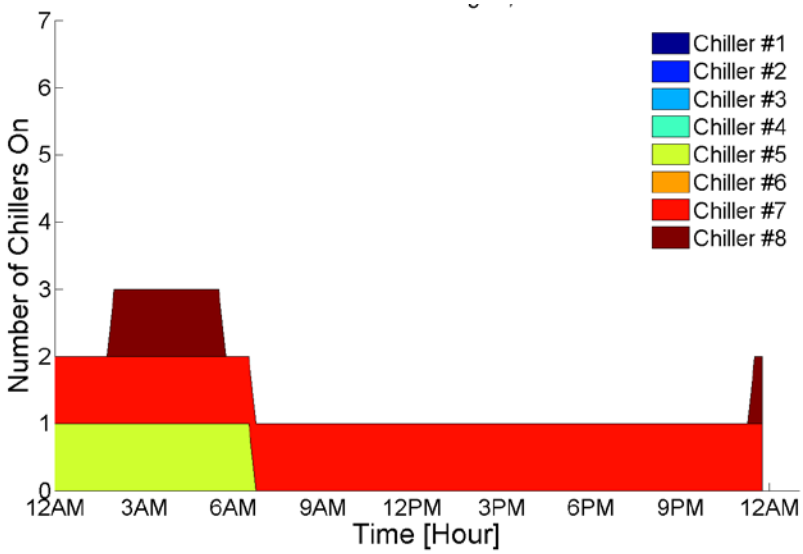

Note: Chiller online status is '1' while off-line is '0'

Figure 54: Simulated Novel Dispatch Chillers to Displace Electrical Load during CPP Window for August 18, 2010

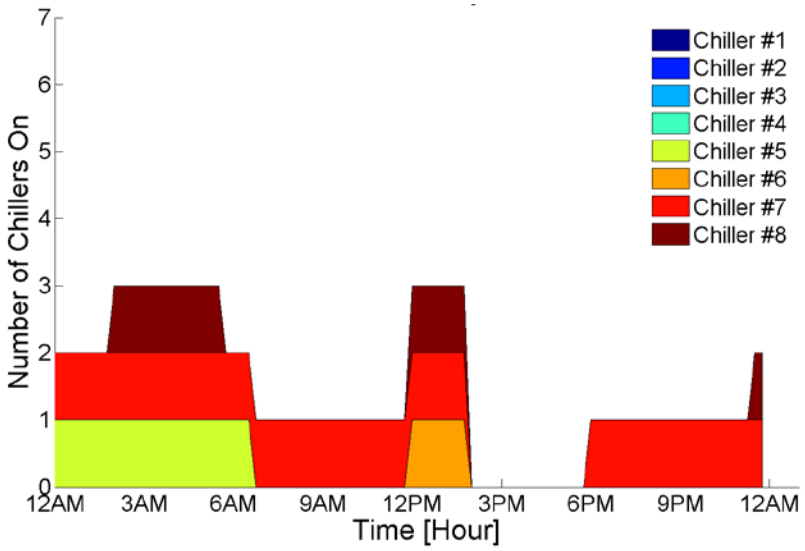

Note: Chiller online status is '1' while off-line is '0'

Figure 55: Business-as-Usual Operation of Chillers for the Selected CPP Day of August 24, 2010

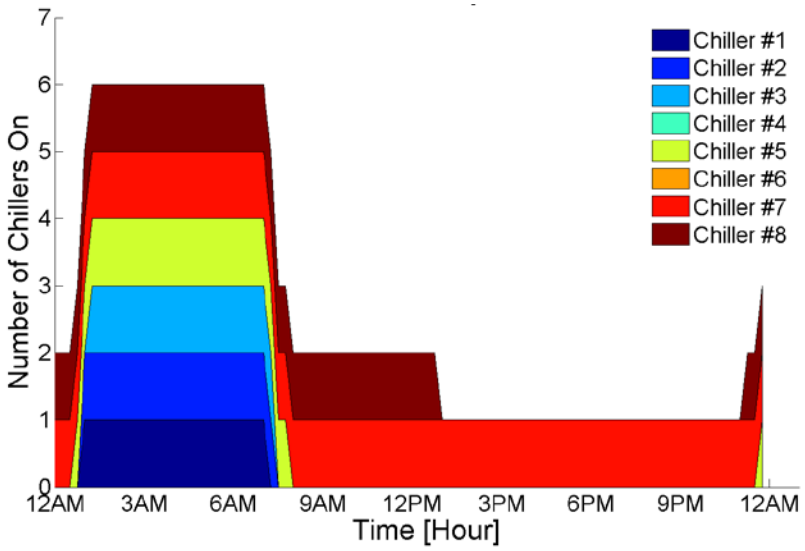

Note: Chiller online status is '1' while off-line is '0'

Figure 56: Simulated Novel Dispatch Chillers to Displace Electrical Load during CPP Window for August 24, 2010

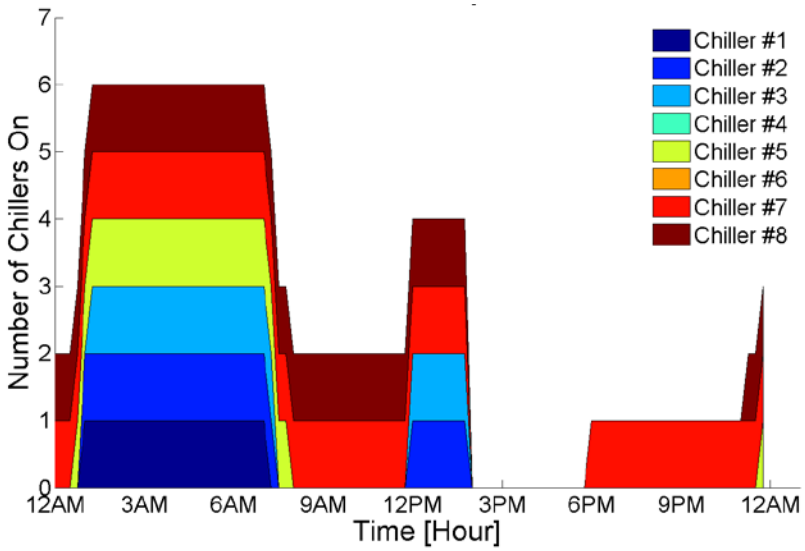

Note: Chiller online status is '1' while off-line is '0'

Figure 57: Business-as-Usual Operation of Chillers for the Selected CPP Day of August 25, 2010

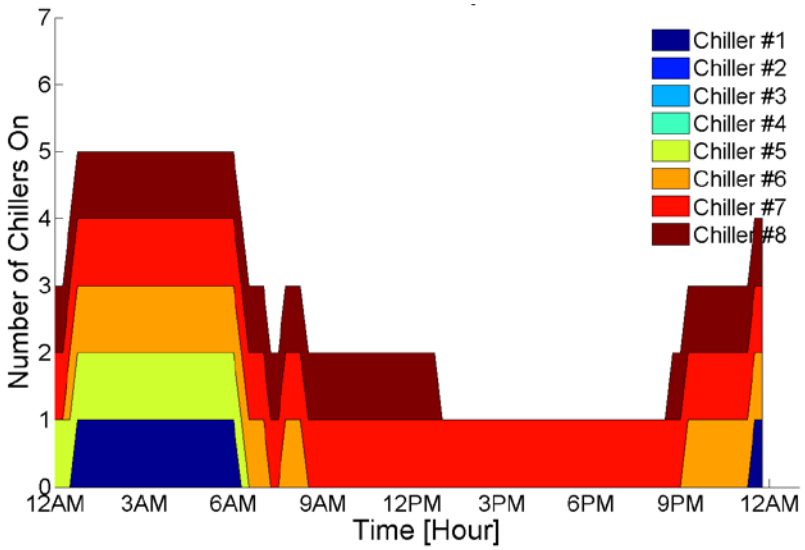

Note: Chiller online status is '1' while off-line is '0'

Figure 58: Simulated Novel Dispatch Chillers to Displace Electrical Load during CPP Window for August 25, 2010

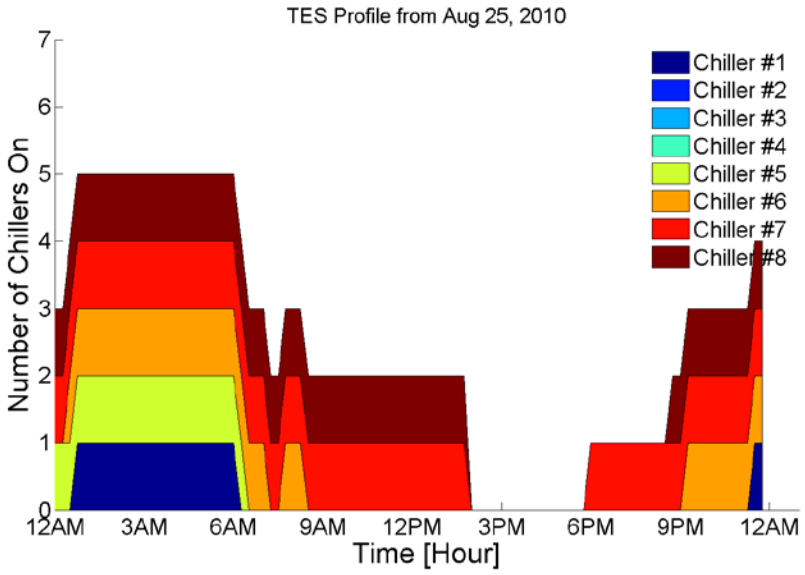

Note: Chiller online status is '1' while off-line is '0'

Figure 59: Business-as-Usual Operation of Chillers for the Selected CPP Day of August 26, 2010

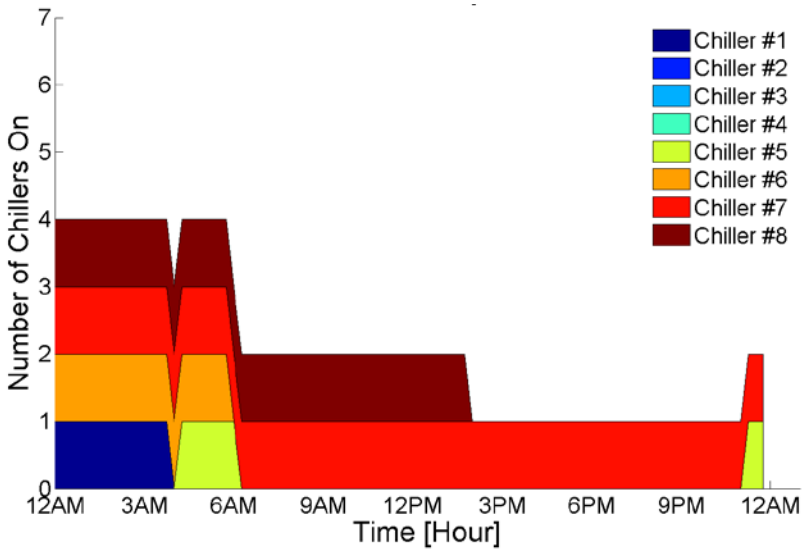

Note: Chiller online status is '1' while off-line is '0'

Figure 60: Simulated Novel Dispatch Chillers to Displace Electrical Load During CPP Window for August 26, 2010

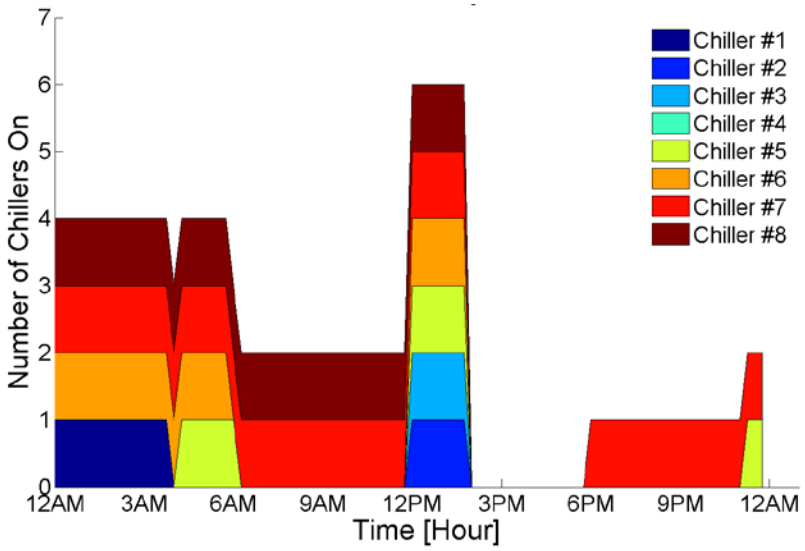

Note: Chiller online status is '1' while off-line is '0'

Figure 61: Business-as-Usual Operation of Chillers for the Selected CPP Day of September 3, 2010

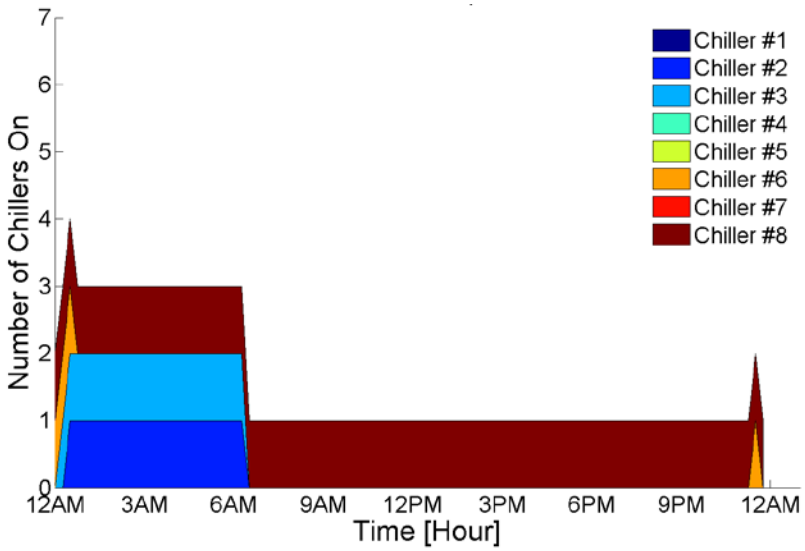

Note: Chiller online status is '1' while off-line is '0'

Figure 62: Simulated Novel Dispatch Chillers to Displace Electrical Load during CPP Window For September 3, 2010

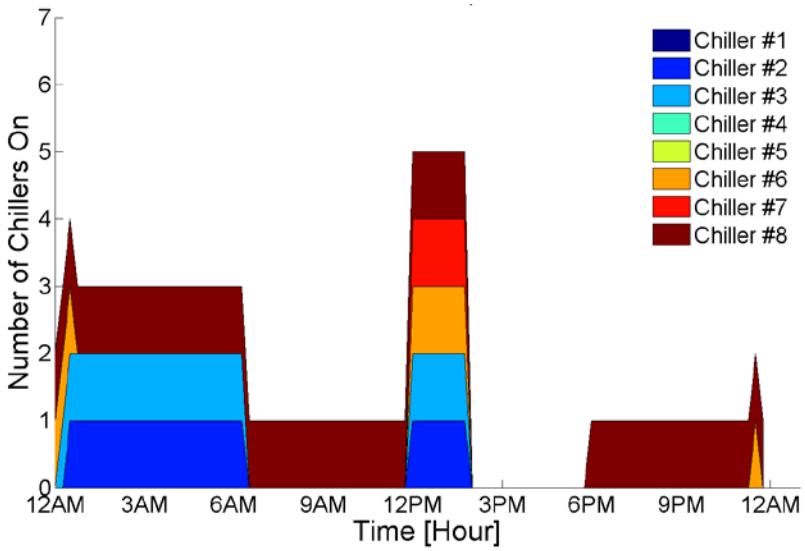

Note: Chiller online status is '1' while off-line is '0'

Figure 63: Business-as-Usual Operation of Chillers for the Selected CPP Day of September 29, 2010

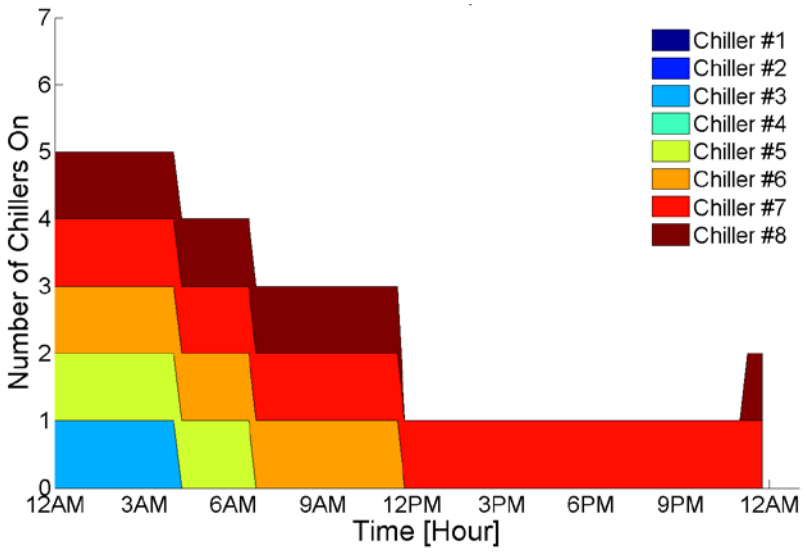

Note: Chiller online status is '1' while off-line is '0'

Figure 64: Simulated Novel Dispatch Chillers to Displace Electrical Load during CPP Window for September 29, 2010

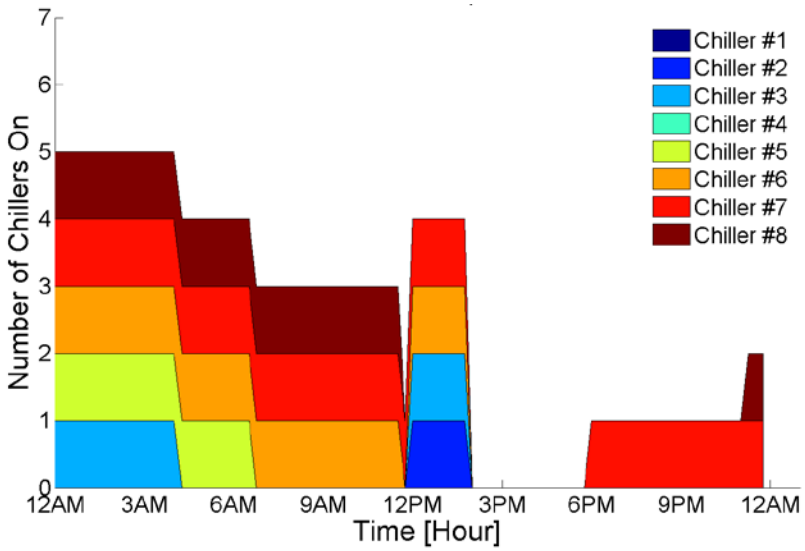

Note: Chiller online status is '1' while off-line is '0'

Figure 65: Business-as-Usual Operation of Chillers for the Selected CPP Day of September 30, 2010

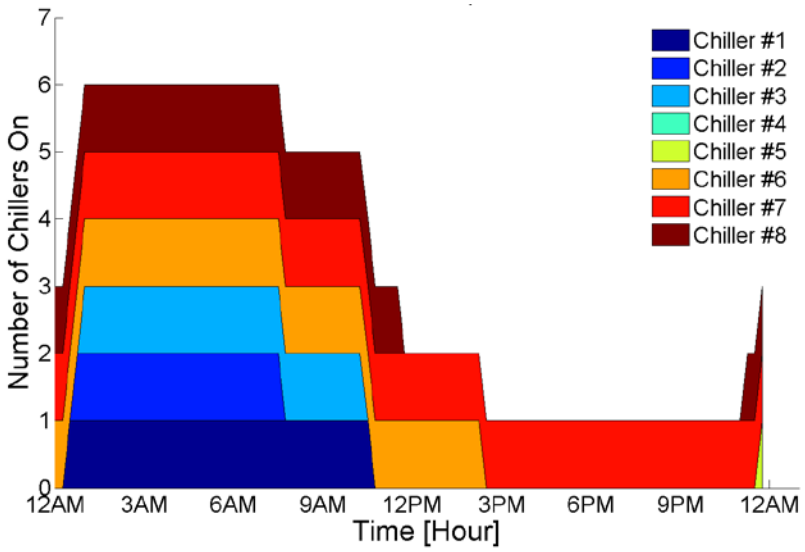

Note: Chiller online status is '1' while off-line is '0'

Figure 66: Simulated Novel Dispatch Chillers to Displace Electrical Load during CPP Window for September 30, 2010

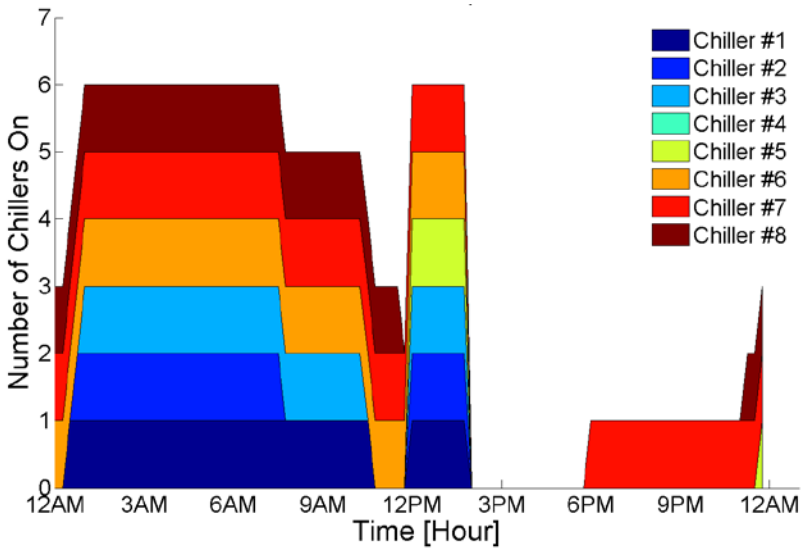

Note: Chiller online status is ‘1’ while off-line is ‘0’

CHAPTER 6:
Technology Transfer and Production Readiness

6.1 Technology Transfer

The purpose of this project is to develop novel control strategies for dynamic economical dispatch of CHP/CCHP systems with emissions constraints and thermal load following capability. The project is specifically designed to focus efforts on enable the use of CHP/CCHP in under-utilized applications. With the emergence of technologies that can efficiently convert heat into cooling (e.g., absorption chilling technology) the consideration of combined cooling, heating and power (CCHP) offers additional market opportunities that are of interest and can significantly contribute to meeting Industrial Technology Program goals. This Chapter will serve as the starting point for the development of a detailed business plan that can begin to be implemented.

6.1.1 Product Overview

The project determined the feasibility of dispatching a microturbine generator using different economic control strategies, reducing the cost of energy to the facility. With the outcomes and conclusions of this project, subsequent research and development can focus on the integration and optimization of the CCHP and application of research findings to various buildings and utility rate structures. This would likely be further followed by studies of scale-up, commercial viability and marketability of products that implement this technology to produce useful products for California and U.S. electric market.

6.1.1.1 Product Description

The Siemens Corporate Research, the subcontractor for this project, has developed the economical dispatch of CCHP systems novel control algorithms, to achieve dynamic economical dispatch of CHP/CCHP systems with emissions constraints and thermal load following capability. These algorithms are executed by the equipment controllers as component of the control system; therefore they are not complete end-use products, but software enhancements for control application programs.

6.1.1.2 Function and Features

The novel control algorithms and architectures that were developed were also demonstrated to dispatch a microturbine generator in the Engineering Laboratory Facility of the University of California, Irvine. The control algorithms were translated to Siemens controls and were installed to demonstrate the novel control algorithms for economical dispatch of a CCHP system. Implement the control algorithm developed in the course of this project, the product needs include: weather forecast for energy demand forecasting, historical energy consumption data for the building, historical data on industrial load activity for model calibration and forecasting on industrial loads activities, access to the building automation for control of the HVAC system, access to the Micro-Turbines to controller. The access to these subsystems can be done with the use of existing software interfaces and building new ones.

6.1.2 Business Case and Market Analysis

The first market target could be California residences and industries. Utilities in the state of California, and Southern California Edison in particular, have been quite progressive with regard to the development and use of CCHP technologies. The technical capabilities of CCHP technologies, especially the primary generators (gas turbines and fuel cells) are not assumed to experience any significant technical performance advances in the period in which the current project will proceed. Although much technological advancement may occur and although technology availability may increase during the course of the project, it is not likely that technology advancement will be focused upon a topic (for example, improving load-following capability) that would have significant impact on the novel control systems developed in this proposal. The regulatory framework is also assumed to be just as it is today with a wide variety of policies that govern CCHP installations throughout the various states of the U.S. It is expected, however, that regulatory policies will change in the near future to support technologies, including CCHP, that will have the benefit of reducing greenhouse gas emissions. Changes in regulatory processes could affect both emissions regulatory bodies as well as utility regulation. All of these possible regulatory changes must be accounted for in the development process with control strategies made flexible enough to accommodate change.

6.1.2.1 Major End-User Market Size

The primary market sector that the research and development products will be applied is the light industrial market sector. Secondary market sectors are the larger commercial and institutional market sectors. The total industrial market for combined cooling, heating and power is substantial and well recognized. Various estimates of the CCHP market potential in the industrial sector are in the range of 30-90 gigawatts (GW) of electrical capacity in the U.S. [see e.g., Resource Dynamics Corporation, 2003; ONSITE SYCOM, 2000] Most studies also identify gas turbine technologies as leading candidates for near-term CCHP applications in the industrial market, so the focus of the proposed effort is reasonable. The "light" industrial market is defined here as less than 20 MW of electrical capacity.

This light industrial market is currently expected to comprise only a small portion of the overall industrial CCHP market penetration. This is expected even though there is significant market potential in this light industrial size class. For example, Resource Dynamics Corporation estimates that more than 2/3 of the total industrial CCHP market potential is comprised of applications less than 20 MW. [Resource Dynamics Corporation, 2003] This is because of several factors, which include the barriers already identified as: (a) lack of cost-competitive options in this size range, (2) lack of information on the value presented by these smaller systems for potential user, and (3) lack of controls sufficient to deal with the highly dynamic nature and relative non-coincidence of the thermal and electrical loads in many of these light industrial applications. The project directly addresses these barriers and significantly contributes to increased market penetration in the light industrial sector. The project team estimates that a 20% improvement in market penetration in the light industrial sector will be facilitated by the products that evolve from the project alone.

In addition, the team expects that similar increased CCHP market penetration can be enabled in the commercial and institutional sectors with the novel control products that result from the project. These markets have been estimated to be as large as 75 GW of electrical capacity in the U.S. [ONSITE SYCOM, 2000] However, the majority of these markets is less amenable to CCHP applications due to more highly variable loads, lower total energy costs per unit of productivity, less coincidence of thermal and electrical loads, more highly dynamic loads, etc. Thus, the team estimates a lower contribution to the CCHP market in the commercial and institutional sectors of 12% that will be facilitated by the products that evolve from the project.

6.1.2.2 Industrial Market

The total new installed capacity due to the advancements proposed herein is estimated using the following equation:

*New CCHP installed capacity = (fraction attributable to proposed technology) * (total industrial market potential) *(CA market fraction) * (fraction of market targeted)*

With a 20% improvement in market penetration in the industrial CCHP market attributed to the technology developed in this proposal, between 1,000 and 4,000 MWe (megawatts of electric capacity) of new CCHP systems will be installed in California [= 0.2* (30 to 90 GW) *(0.25) * 2/3 industrial]. Even if this is limited to those applications between 0.5 – 5MWe the Resource Dynamics study [2003] suggests that this portion of the light industrial market is between 66% (current case) and 85% (future case). Thus the range of potential installed CCHP capacity in the 0.5 – 5MWe size classes due to the technology proposed is 670 –3,400MWe. If one assumes that the typical installation in the light industrial market is 1 MWe, then the total number of installations in the industrial market sector that are enabled by the novel control technology developed will be between 670 and 3,400 installations.

6.1.2.3 Commercial and Industrial Markets

The commercial and institutional CCHP market is estimated to be as large as 75 GW of total market potential [ONSITE SYCOM, 2000]. The team uses the same means of estimating the total new installed capacity due to the advancements proposed herein, but, assumes only a 12% improvement in market penetration due to the product developed in the commercial and institutional sector. Thus, using the following equation:

*New CCHP installed capacity = (fraction attributable to proposed technology) * (total commercial and institutional market potential)* (CA market fraction)*

a 12% improvement in market penetration in the commercial and institutional CCHP market sector leads to 2,250MWe of installed capacity [= 0.12* (75 GW)* (0.25)]. Assuming a typical installation is 1 MWe, then the total number of installations in the commercial and institutional market sectors will be 2,250 installations.

6.1.3 Public Benefits

Public benefits will be realized in at least three areas: (1) energy savings, which will impact the longevity of limited primary energy reserves and the cost of energy supply, (2) criteria pollutant

emissions reductions, which will improve air quality, and (3) greenhouse gas emissions reductions, which will reduce our impact on the global climate.

6.1.3.1 Energy Savings

The combined estimate of increased market applications of CHP/CCHP technology in the light industrial, commercial and institutional markets is between 2,920 and 5,650 MW. Assuming that these systems have an average electrical efficiency of 36% and that 50% of the useful heat produced is recovered to replace a boiler, then a total mixed (heat and power) CCHP system efficiency of 68% is achieved. Comparing this to a current average for grid supplied electricity of 33% and a 95% efficient boiler and assuming a 90% capacity factor for the CCHP systems can save in the range of 9.9 – 29.6TBtu/year due to the technology proposed. This was estimated by summing the results from the following expressions:

*Electrical energy savings/year = (efficiency difference) * (installed capacity, MW) * (capacity factor) * (8766 hours/year) * (3.412E-6 TBtu/MW-hour)*

*Thermal energy savings/year = (recovered fraction) * (installed capacity, MW) * (capacity factor) * (8766 hours/year) * (3.412E-6 TBtu/MW-hour) / (boiler efficiency)*

Interestingly, the energy savings estimate is not very sensitive to the assumed electrical efficiency of the CCHP system. For example with all of the same assumptions except for an increase in average CCHP electrical efficiency up to 40%, annual energy savings is estimated to be in the range of 10.4 – 31.2TBtu/year.

6.1.3.2 Criteria Pollutant Emissions

The proposed effort will lead to significant energy savings in the light industrial, commercial and institutional sectors. The average NOx emissions intensity of electricity provision and natural gas boilers is 0.2 kg NOx/MWh and 0.014 kg NOx/MMBtu, respectively. Thus, the proposed effort is expected to reduce NOx criteria pollutant emissions by roughly between 177 to 531 metric tons of NOx per year.

6.1.3.3 Greenhouse Gas Emissions

In addition, the carbon dioxide (the primary greenhouse gas) emissions intensity of electricity provision and natural gas boilers is 608.2 kg CO_2/MWh and 53.5 kg CO_2/MMBtu, respectively. As a result, the proposed effort is expected to contribute to reductions in carbon dioxide emissions of roughly 0.63 to 1.89 million metric tons annually. Thus, the proposed effort will significantly contribute to reducing the California carbon intensity and contributing to state goals for reduction of greenhouse gas emissions.

6.1.4 Product Development Status and Needs

6.1.4.1 Product Development Status

In this project, physical models of CCHP system components were developed and the economic and environmental analyses strategies were developed. Economic dispatch strategies have been developed and these dispatch strategies can enable Combined Cooling, Heat and Power (CCHP) technologies to reduce overall facility energy costs. The control algorithms and

architectures were developed and translated to Siemens controls and were installed to demonstrate the novel control algorithms for economical dispatch of a CCHP system.

6.1.4.2 Remaining Steps

Before the economical dispatch tools are market ready, robust sets of threshold control parameters, suitable for use with site-specific configurations must be determined. Determining these sets of parameters is out of the scope of the current project. More work is also needed to complete development of the user interface for the economical dispatch tool.

6.1.5 Technology Transfer Actions

6.1.5.1 Manufacture Commitment

There is one participating manufacture (Siemens). The major commercialization partner in this project is Siemens Corporate Research (SCR). SCR works closely with Siemens Building Technologies (SBT). SCR and SBT have significant previous experience and capabilities to translate the novel controls to application software. Significantly, Siemens has applied Model Reference Adaptive Control (MRAC) for Heating Ventilation and Air-conditioning (HVAC), developed a Green Resource Advisor to help end-users design, operate and retrofit their building systems to include "Green Components," and developed distributed optimization and machine learning techniques for building automation and control entitled "Total Plant Optimization."

6.1.5.1 Purchase Incentive

The energy savings and benefits of the results of this project are not dependent upon any code requirements. However, any incentives (e.g., rebates, direct incentives, code recommendations, or points, etc.) will increase the appeal of novel control of CCHP system, both to potential buyers and manufactures.

6.1.5.1 Educating CCHP Engineers and Designers

In current practice, energy managers, architects, commercial building owners, businesses, etc. are not aware of the benefits that CHP/CCHP technology can provide. It is necessary to educate these individuals on the existence, general principals, and benefits of CCHP system and the economical dispatch of a CCHP system. Two articles were submitted to the Journal of Power Sources which will be dedicated to the topics. Case studies of various buildings of this project could be also made available as well.

6.2 Production Readiness

The simulations and demonstration in this project has indicated that the economical dispatch of CCHP system holds the promise of becoming the besting performing control system in the industrial and commercial markets. The technology is on the verge of being commercialized. To determine the steps that will lead to the manufacturing of the technologies developed in this project or to the commercialization of the project's results, a Production Readiness Plan is determined.

6.2.1 Production Process and Current Facilities

The control system for economical dispatch of CCHP system consists of several components: Siemens Smart Energy Box, weather forecast module, demand management module, optimization module. The Siemens Corporate Research has developed the components in the economical dispatch of CCHP systems novel control system, to achieve dynamic economical dispatch of CHP/CCHP systems with emissions constraints and thermal load following capability. These algorithms are executed by the equipment controllers as component of the control system and such software enhancements for control application programs are ready to launch. The Siemens Smart Energy Box is manufacture by Siemens Corp. and is currently available in the market. Combined with the components developed in this project, the production can be completed.

6.2.2 Required Improvements

Before the economical dispatch tools enter the stage of full production, robust sets of threshold control parameters, suitable for use with site-specific configurations must be determined. Building loads and energy consumption patterns and CCHP systems on-site could be largely different. Therefore determining the sets of parameters in the economical dispatch control strategy is required to improve the product. In addition, improvement in the user interface for the economical dispatch tool is also required.

6.2.3 Cost Estimate and Required Investment

The team estimates that approximately $1 million is required to advance the tools and novel control techniques to commercial deployment.

6.2.4 Full Production Ramp-Up Plan

While the merits of the economical dispatch of CCHP system product have been proven in the simulations and demonstration, a number of steps must be taken before full production levels can be reached. Further optimization of the algorithm must be carried out with more site-specific configurations and control parameters to better accommodate various buildings and facilities.

GLOSSARY

Term	Definition
EPIC	Electric Program Investment Charge
CHP	Combined Heat and Power
SCE	Southern California Edison
DG	Distributed Generation
TOU	Time of Use
SCG	Southern California Gas Company
MUD	Maximum Utility Demand
ICBA	Installed Capacity versus Building Average
ICBM	Installed Capacity versus Building Maximum
CARB	California Air Resources Board
SEB	Smart Energy Box
CRC	Capacity Reservation Charge
EPA	Environmental Protection Agency
MTG	Microturbine Generator
HR	Heat Recovery
kW	Kilowatt
kWh	Kilowatt-Hour
NEI	National Emissions Inventory
O&M	Operations and Maintenance
SGIP	Self-Generation Incentive Program
NFCRC	National Fuel Cell Research Center
UCI	University of California, Irvine

REFERENCES

Flores, Robert. Control of Dispatch Dynamics for Lowering the Cost of Distributed Generation in the Building Environment. University of California, Irvine. Master Thesis, 2013.

Resource Dynamics Corporation, *Cooling, Heating, and Power for Industry: A Market Assessment*, Prepared for the U.S. Department of Energy, 2003.

ONSITE SYCOM Energy Corporation, The Market and Technical Potential for Combined Heat and Power in the Commercial/Institutional Sector, Prepared for U.S. Department of Energy, 2000.